BIOANALYTICAL CHEMISTRY OF MICROTUBULE STABILIZERS: PROTEOMIC CHANGES INDUCED BY MT STABILIZER IN NON-SMALL CELL LUNG CANCER (NSCLC) CELLS

by

Ying Lu

B.S., Nankai University, 1995

M.S., Rensselaer Polytechnic Institute, 2002

Submitted to the Graduate Faculty of

Arts and Sciences in partial fulfillment

of the requirements for the degree of

Master of Science

University of Pittsburgh

2005

UNIVERSITY OF PITTSBURGH

FACULTY OF ARTS AND SCIENCES

This thesis was presented

by

Ying Lu

It was defended on

April 13, 2005

and approved by

Steve Weber, PhD, Professor

Kazunori Koide, PhD, Assistant Professor

Billy W. Day, PhD, Associate Professor

Thesis Director: Billy W. Day, PhD, Associate Professor

BIOANALYTICAL CHEMISTRY OF MICROTUBULE STABILIZERS: PROTEOMIC CHANGES INDUCED BY MT STABILIZERS IN NON-SMALL CELL LUNG CANCER (NSCLC) CELLS

Ying Lu, MS

University of Pittsburgh, 2005

Lung cancers are typically malignant tumors found in one or both lungs. These cancers usually form from cells that line the airways and nearby glands because it is these cells that come into contact with the air we breathe and the many carcinogens that are contained within it. In the US, there are approximately 413,000 people with lung cancer at any given time. Non-small cell lung cancer accounts for about 80% of all lung cancer cases. So far, the diagnosis of lung cancer relies significantly on physical examination. This late detection usually results in a high probability of metastasis and consequently high mortality. Therefore, as the second most common cancer diagnosed in US, the earlier detection and therefore treatment of lung cancer has been one of the primary goals of researchers.

Paclitaxel (Taxol), a microtubule (MT) stabilizing agent originally noted to be useful against ovarian and breast cancers, has recently been found to have clinical utility in the treatment of lung cancer. A variety of structurally diverse MT stabilizers have been discovered over the past decade. These agents include discodermolide, laulimalide and dictyostatin, originally isolated from marine sponges, epothilones, originally isolated from the broth of fermenting soil bacteria, and eleutherobin, first found from soft corals. Many reports show that these agents have activity, all in vitro and some in vivo, against human cancers. Their working mechanism includes the

enhancement of tubulin assembly into hyperstable microtubules, the G2/M arrest of cells, and the induction of apoptosis. As the MT stabilizing action leads to the induction of apoptosis, there obviously must be some changes in the affected cells' proteome, including both expression and post-translational changes, which are a result of MT stabilization and represent early signals that lead to activation of the apoptosis cascade. The goal of the project is to detect and characterize the earlier proteomic changes of NSCLC cells after treatment with MT stabilizing agents using 2-D DiGE and MALDI-TOF. It is expected that a more detailed understanding of NSCLC cells' response to MT stabilizers will allow for more rational decision-making in the clinical treatment of diseases.

TABLE OF CONTENTS

LIST OF TABLES

LIST OF FIGURES

ABBREVIATIONS

ATP: adenosine triphosphate
CBB: Coomassie Blue Brilliant
CHCA: α-cyano-4-hydroxycinnamic acid
DCD: discodermolide
DMSO: dimethylsulfoxide
DSS: dissuccinimidyl suberate
DTT: dithiothreitol
EDTA: ethylenediaminetetraacetitic acid
EGTA: ethyleneglycotetraacetic acid
EHNA: erythro-9-(2-hydroxy-3-nonyl) adenine
GFP-GR: green fluorescent protein-glucocorticoid receptor
GDP: guanosine diphosphate
GTP: guanosine triphosphate
HEPES: 4-(2-hydroxyethyl)-1-piperazineethanesulfonic acid
IAA: iodoacetamide
MALDI-TOF/TOF-MS/MS: matrix-assisted laser desorption ionization-time of flight/time of flight-mass spectrometry/mass spectrometry
MAPs: microtubule-associated proteins
MES: 2-[N-morpholino]- ethane sulfonic acid
MOPS: 3-morpholinopropanesulfonic acid
MTS: 3-(4,5-dimethylthiazol-2-yl)-5-(3-carboxymethoxyphenyl)-2-(4-sulfophenyl)-2H-tetrazolium
MTT : 3-(4,5-dimethlythiazol-2-yl)-2,5-diphenyltetrazolium bromide
MT(s): microtubule(s)
PI: protease inhibitors
PIPES: piperazine-N,N'-bis(2-ethanesulfonic acid)
PMSF: phenylmethylsufonyl fluoride
PVDF: polyvinylidene difluoride
QSAR: quantitative structure-activity relationship
SARs: structure-activity relationships
SDS-PAGE: sodium dodecyl sulfate-polyacrylamide gel electrophoresis
TGS: Tris-Glycine-SDS
2D DiGE: two dimensional differential gel electrophoresis

1. INTRODUCTION

The pharmacology of drug discovery includes two main categories. Rational drug design is based on biochemical assays that lead to structure-activity relationship (SAR) between the test agent molecules and the biological target, and includes computational molecular modeling based on the structure of the target (if known) and the structures of the test agents. Cell based drug design uncovers new drugs through screening of compounds for their biological effect on target function (i.e., test agent-induced change in phenotype). Though cell-based readout systems are not as straightforward as the former, the method has shown its importance and is becoming a mainstream strategy employed by researchers, mainly because, unlike the former, the cell-based systems give a readout of the test agents' activities in living cells. The work done by Issaeva *et al*. on the isolation of a new p53 activator with anticancer properties is one of the successful examples from the cell-based strategy [1, 2]. The overall objective of this project is to develop an early stage and high information content cell-based screening system for microtubule stabilizing agents, with particular emphasis on use of proteomics technologies. Through wise selection of screening strategies and detection methods, novel anti-carcinoma agents with potential of clinical application could be found. In addition, the large amount of data from the screening process will provide useful information of biological targets, and therefore help gain an understanding of the working mechanism of the drugs.

1.1. HYPOTHESIS AND SPECIFIC AIMS

A common feature in the working mechanism of different MT stabilizers includes their enhancement of tubulin assembly into hyperstable microtubules, the arrest of cells in the G2/M phase of the cell cycle, and the induction of apoptosis [3]. The hypothesis is that as the MT stabilizing action typically leads to the induction of apoptosis, there are detectable, signature changes in the affected cells' proteome. The possible changes as a result of MT stabilization include both protein expression levels and post-translational changes, and will represent early signals that lead to activation of the apoptosis cascade.

The specific aims therefore are to (1) Determine the antiproliferative activity of microtubule stabilizing agents on human cancer cell lines; (2) Detect the early stage proteomic changes induced by microtubule stabilizers; (3) Identify the biological targets; and (4) Explore the mechanism of microtubule stabilizers on human carcinoma cells.

1.2. BACKGROUND

1.2.1. Microtubules and MAPs

Microtubules (MTs) are intracellular tubes of regular circumference that form cytoskeletal lattices and the mitotic spindle. They are built and dismantled from the dynamic assembly/disassembly of heterodimers of the ~50kDa proteins α- and β- tubulin, of which several isotypes for each monomer exist in mammalian systems [4] (Figure 1).

Microtubule dynamics encompasses the multiple reactions involved in the rapid assembly and disassembly of microtubules, particularly those forming the spindle. There are two interesting

kinds of dynamic behaviors, dynamic instability and treadmilling. The former is a process in which the individual microtubule ends switch between phases of relatively slow sustained growth and rapid shortening [5]. The latter is the net growth at one microtubule end and the net shortening at the opposite end [6]. Many cellular activities, including normal cell division, intracellular transport, cellular motility, cell signaling and maintenance of cell shape are all dependent on the highly regulated dynamic instability process of the tubulin/microtubule system [7]. Therefore, the tubulin/microtubule complex has proven to be a clinically useful antitumor target. The examples of chemotherapeutics that act via perturbation of tubulin polymerization include paclitaxel (Taxol®), docetaxel(Taxotere®), vinblastine and discodermolide [8-11] (Figure 2). Docetaxel is a semi-synthetic derivative of paclitaxel. Unlike the other three compounds, which stabilize microtubules, vinblastine aggregates tubulin and leads to microtubule depolymerization.

There are a large group of microtubule-associated proteins (MAPs) [12] that bind the microtubules, acting mainly to stabilize them against disassembly. The binding of MAPs to microtubules is largely dependent on MAP phosphorylation status, making them targets for protein kinases. MAPs are tissue and cell type specific. Major MAPs include MAP1, MAP2, and MAP4 with molecular weights of 200-300 KDa, and the neuronal protein tau (20-60 KDa). MAP4 is the most abundant and ubiquitous MAP in non-neuronal cells; it stabilizes microtubules [13].

Figure 1: Illustration of microtubule structure. The microtubule is formed as series of protofilaments via the noncovalent attachment of tubulin dimers to the plus (growing) end of the microtubule.

1.2.2. Microtubule stabilizing agents

Paclitaxel (Taxol®), a natural product isolated from Pacific yew tree, *Taxus brevifolia*, is a microtubule (MT) stabilizing agent that has demonstrated significant clinical success. It was originally noted to be useful against ovarian and breast cancers. Recent studies show that it also has clinical utility in the treatment of lung cancer [14, 15]. A variety of structurally diverse MT stabilizers have been discovered over the past decade. These agents include discodermolide, laulimalide and dictyostatin-1, originally isolated from marine sponges [11,16-19], epothilone B, originally isolated from the broth of fermenting soil bacteria [20], and eleutherobin, first found

from soft corals [21] (Figure 2). Many reports show that these agents have activity, all in vitro and some in vivo, against human cancers. Even though the binding site of laulimalide on MTs differs from the other MT stabilizers [22], these agents have a common feature in that their working mechanism includes enhancement of tubulin assembly into hyperstable microtubules, the arrest of cells in G2/M phase of the cell cycle and the induction of apoptosis.

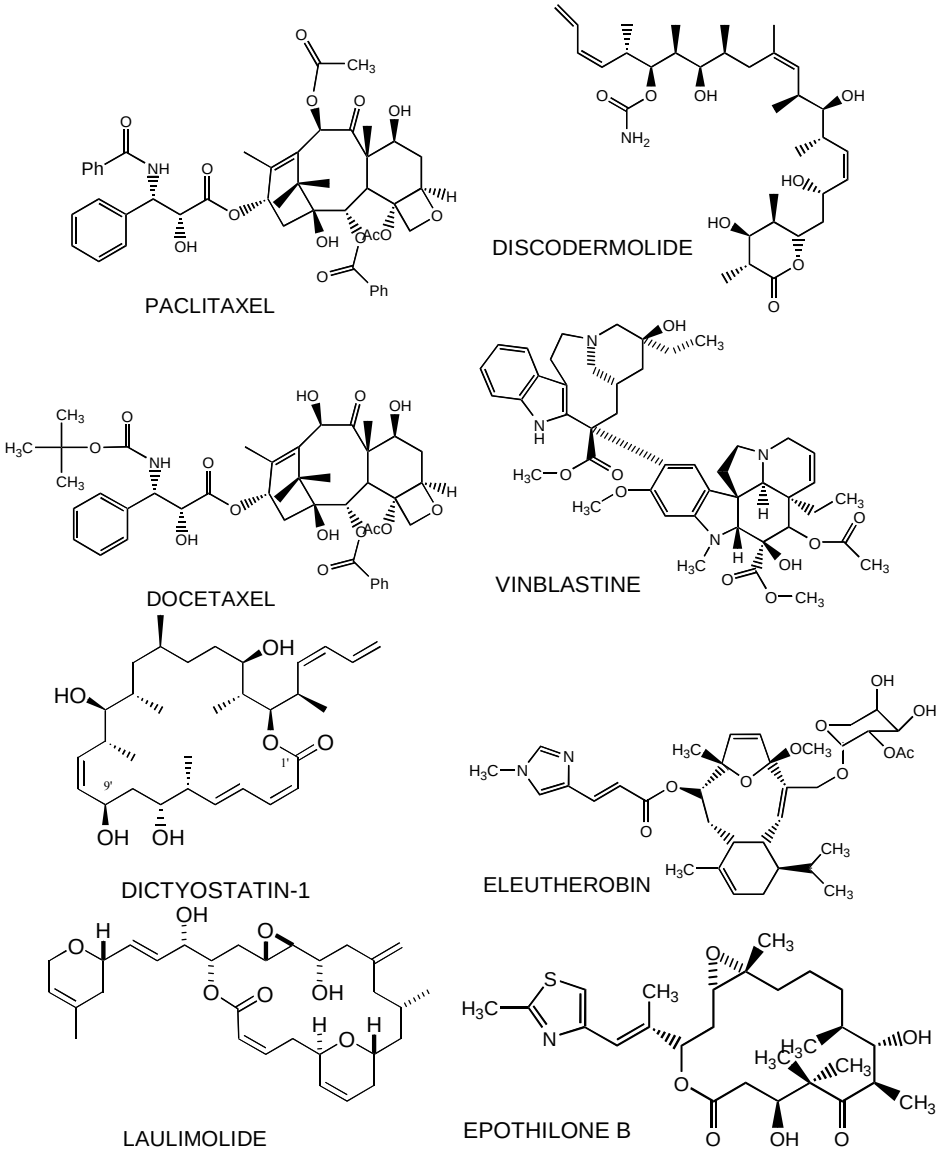

Figure 2: Chemical structures of the microtubule polymerization inhibitor vinblastine and the depolymerization inhibitors paclitaxel, docetaxel, discodermolide, laulimalide, dictyostatin-1, eleutherobin and epothilone B.

1.2.3. Working mechanism of MT stabilizing agents

It is well known that paclitaxel binds to microtubules in cells and arrests cells in mitosis by stabilizing mitotic spindle microtubules [23, 24]. This differs from the many agents discovered before it (e.g., colchicine, vinca alkaloids), which inhibit tubulin polymerization and cause cellular microtubules to disappear. Photoaffinity studies have indicated that pacliaxel binds to the beta-tubulin subunit at the N-terminal residues 1-31 and 217-233. Electron crystallography of zinc-induced tubulin polymeric sheets has also shown that the binding site of docetaxel and paclitaxel is in the interior surface of the microtubule lumen [25-28]. Other MT stabilizing agents, e.g., discodermolide, laulimalide, dictyostatin and epothilone B, have all been reported that have a similar mechanism of action. Experiments performed independently by different groups show that discodermolide and epothilone B competitively inhibits the binding of [^{3}H]paclitaxel to microtubules. Such an inhibitory pattern implies that these compounds bind at the same (or perhaps an overlapping) site on tubulin as does paclitaxel [29, 30]. This implication is merited by a recent finding by Martello *et al.*, which describes a synergistic cytotoxic activity of discodermolide with paclitaxel against several cancer cell lines [31]. Dictyostatin also binds to the same site on microtubules as does paclitaxel. [Madiraju *et al.*, submitted] Shin *et al*. have reported the synthesis and antiproliferative effects of cyclic discodermolide analogs resembling the structure of dictyostatin. The structural similarity between these two agents strongly suggests that they share a common binding site on tubulin [32]. A similar competition assay on laulimalide was reported by Pryor *et al*.. The results show that laulimalide is unable to inhibit the binding of [^{3}H]paclitaxel or of 7-*O*-[*N*-(2,7-difluoro-4'-fluoresceincarbonyl)-L-alanyl]paclitaxel, a fluorescent paclitaxel derivative, to tubulin. This indicates that laulimalide, while as active as

paclitaxel in promoting cold-stable microtubule spindles, binds to a distinct site on tubulin polymer [22]. Currently, a combined strategy of photoaffinity labeling with proteomic method is being employed to investigate the laulimalide binding site on microtubules in the Nelson and Day groups.

2. RESEARCH METHODS AND PRELIMINARY RESULTS

2.1. ANTIPROLIFERATIVE ACTIVITY OF MICROTUBULE STABILIZING AGENTS

2.1.1. Introduction

Antiproliferative assays are widely used to evaluate new agents against carcinoma cells and are a part of the drug discovery process. Three microtubule stabilizing agents on hand in the Day group were assessed for antiproliferative and potential cytotoxic activity against a panel of human carcinoma cells. Six well-established carcinoma cell lines were examined in this assay: MDA-MB231 (breast), PC3 (prostate), 2008 (ovarian), 1A9 (ovarian), 1A9/Ptx10 and 1A9/Ptx22 (ovarian with beta tubulin mutation). These cell lines were chosen in part because they all are well-studied in the Day lab. Moreover, these cancer types represent a large percentage of solid tumors currently reported in the U.S.A. These cell lines have similar growth characteristics and are particularly sensitive to antimitotic agents.

The MTS [3-(4,5-dimethylthiazol-2-yl)-5-(3-carboxymethoxyphenyl)-2-(4-sulfophenyl)-2H-tetrazolium] assay is a colorimetric method for determining the number of viable cells in proliferation or cytotoxicity assays. In this assay, the MTS tetrazolium compound is reduced by cells' mitochondria into a colored formazan product that is soluble in tissue culture medium [33]. This conversion is presumably accomplished by the NADPH or NADH produced by dehydrogenase enzymes in metabolically active cells [34]. Assays are performed by adding a small amount of the MTS reagent directly to culture wells, incubating for 1 h and then recording absorbance at 490 nm minus that observed at 630 nm with a plate reader. The quantity of

formazan product as measured by the amount of 490 nm absorbance is directly proportional to the number of living cells in culture [35]. The reference wavelength at 630 nm is used to reduce background contributed by excess cell debris, fingerprints and other nonspecific absorbance. The MTS assay is a convenient and fast way to determine the cell numbers, thus helping to determine the antiproliferative activity of the compounds.

2.1.2. Experimental section

2.1.2.1. Materials

RPMI medium 1640, penicillin-streptomycin, L-glutamine, and trypsin-EDTA were obtained from Invitrogen Co., Carlsbad CA. Fetal bovine serum (FBS) was obtained from Hyclone, Logan, UT. Trypan blue solution (0.4%) was obtained from Sigma Co., St. Louis, MO. 96-Well plates were obtained from Corning-Costar, NY. Paclitaxel was from the Drug Synthesis Branch of the National Cancer Institute. Discodermolide was a gift from Novartis Pharmaceutical Co., Laulimalide and dictyostatin were provided, respectively, by Scott Nelson's and Dennis Curran's group at the University of Pittsburgh. MDA-MB231, PC3 and 2008 cells were from the ATCC. The 1A9 cells and their paclitaxel-resistant clones were gifts from Drs. Tito Fojo and Paraskevi Ginnakakou at the National Cancer Institute.

2.1.2.2. Methods

Cells were grown in RPMI 1640 medium with 10% FBS. Human cancer cells were trypsinized and plated into 96-well microtiter plates at 500-2000 cells/well (depending on the cell line), allowed to attach and grow for 48 h, and then treated with vehicle (DMSO) or test agent for an

additional 72 h. In each case, one plate consisted entirely of cells in medium or medium alone to determine time zero cell numbers. The other plates in a given determination contained eight wells of control cells, eight wells of medium, and four wells of each agent concentration tested in 5-fold dilutions. Cell viability was determined with the MTS assay and 50% growth inhibitory concentration (GI_{50}) values were estimated and further confirmed by repeating the screen using 2-fold dilutions centered on the initial estimated GI_{50} concentration, again in quadruplicate.

2.1.3. RESULTS AND DISCUSSION

Table 1 shows the effects of the potent microtubule stabilizing agents paclitaxel, discodermolide, laulimalide and dictyostatin on carcinoma cell growth. All of the compounds displayed potent antiproliferative activity against human carcinoma cell lines. Compared to paclitaxel, discodermolide is less potent toward cancer cells and the GI_{50} values of both are almost within the same order of magnitude. Laulimalide is apparently the most potent of the compounds. The data show that it is almost two orders of magnitude more potent than discodermolide. Due to the interesting and encouraging results, laulimalide was further tested against the 1A9 human ovarian cancer cell lines and their palcitaxel-resistant clones, 1A9/Ptx10 and 1A9/Ptx22. Low nanomolar activity was obtained against the two paclitaxel-resistant cell lines 1A9/Ptx10 and 1A9/Ptx22. Similar results has been reported by Pryor, *et al*. in Hamel's group [22] (Table 2). The cytotoxicity of laulimalide was examined with a series of human ovarian cancer cell lines in comparison with paclitaxel and epothilone A and B. Among six cell lines, A2780/AD10 is a multidrug-resistant line that overexpresses P-glycoprotein. 1A9/Ptx10 and 1A9/Ptx22 are paclitaxel-resistant lines. A8 and B10 are resistant to epothilones A and B, respectively. The latter four lines all have mutations in the M40 β-tubulin gene at amino acid residues near taxoid

binding site [36]. From the data in Table 2, we can see that laulimalide, like epothilones A and B, is not a good substrate for P-glycoprotein, and remains its antiproliferative activity in A2780/AD10 cell line. All four lines with mutation-based paclitaxel/epothilone resistance also retain their sensitivity to laulimalide. This result is obviously an indication that laulimalide binds tubulin assembly at a new site and might have synergistic cytotoxic activity with compounds bound at the taxoid site.

Besides of laulimalide, dictyostatin has also been reported that remain potency in paclitaxel-resistant human cancer cell lines (NCI/ADR-RES and MES-SA/DX5) expressing active P-glycoprotein [37] (Table 3).

Table 1: Antiproliferative activities of a panel of MT stabilizing agents[a]

Compound	GI_{50} (nM) ± SE					
	MDA-MB231	PC3	2008	1A9	1A9/Ptx10	1A9/Ptx22
Paclitaxel	2.4 ± 1.6	15 ±2	9.2 ±1.6	0.71 ± 0.11	64 ± 8	51 ± 9
Discodermolide	16 ± 3	67 ±4	72 ±5	1.7 ± 1.2	6.2±3.6	7.0 ± 8.4
Laulimalide	0.0839 ± 0.0135	0.158 ± 0.011	0.306 ± 0.159	<0.08	<0.08	<0.08
Dictyostatin				0.69 ± 0.80	3.2 ± 2.4	1.3 ± 1.0

[a] MDA-MB231 (human breast cancer cell line); PC3 (human prostate cancer cell line); 2008 (human ovarian cancer cell line); 1A9 (human ovarian cancer cell line); 1A9/Ptx10 (Phe270->Val beta-tubulin mutation); 1A9/Ptx22 (Ala364->Thr beta-tubulin mutation).

Table 2: Cytotoxic activity of laulimalide in paclitaxel or epothilones resistant human ovarian cell lines [excerpted from Pryor et al., ref. 22]

Compound	IC_{50} (nM) ± SE					
	1A9	PTX10	PTX22	A8	B10	A2780/AD10
Laulimalide	3.9 ± 0.4	6.0 ± 1	6.3 ± 1	9.2 ± 2	15 ± 0.2	31 ± 0.6
Epothilone A	1.7 ± 0.3	18 ± 7	4.3 ± 1	93 ± 30	125 ± 25	16 ± 0.6
Epothilone B	0.17 ± 0.08	0.70 ± 0.4	0.32 ± 0.2	6.4 ± 4	9.0 ± 5	2.6 ± 2
Paclitaxel	1.7 ± 0.3	50 ± 11	34 ± 3	13 ± 2	16 ± 4	4000 ± 900

Table 3: Cytotoxic activity of dictyostatin and paclitaxel in human cancer cell lines following 72-hr exposure to the test agents [excerpted from Isbrucker et al., ref. 37]. (Values in brackets are relative fold resistance, indicating the reduced potency of the compound in the resistant cell lines.)

Cell line	IC_{50} (nM) ± SE	
	Dictyostatin-1	Paclitaxel
A549	0.95 ± 0.25	5.13 ± 2.9
MCF-7	1.5 ± 0.9	2.5 ± 0.7
NCI/ADR-RES	20 ± 4.2 (13×)	3331 ± 652 (1332×)
MES-SA	4.1 ± 1.4	3.3 ± 0.6
MES-SA/DX5	11 ± 2.4 (3×)	1654 ± 230 (501×)

2.2. PROTEOMIC CHANGES INDUCED BY MICROTUBULE STABILIZING AGENTS

2.2.1. Introduction

The hypothesis to be tested in the present work is that because the MT stabilizing action well proceeds the induction of apoptosis, there must be some changes in the proteome of the affected

cells, including both expression level and post-translational changes. Significant changes in the proteome of breast cancer cells treated with MT stabilizers have been shown in the literature to become apparent after a long time of treatment [38]. Few proteomic changes have yet to be detected in the shorter treatment times. In this study, human non-small cell lung cancer cell line H460 was selected with a short treatment time (6 h).

The experimental work flow was designed to consist of eight parts as shown in Figure 3, including cell culture, treatment of cancer cells with drugs for different time periods, cell lysis and protein clean-up, labeling of control and drug treated samples with electrophilic fluorescent dyes (staining) and separation of a treated sample combined with its vehicle control cell sample by 2D gel electrophoresis, gel image acquisition and analysis, protein identification by modern mass spectrometry (e.g., MALDI-TOF/TOF-MS/MS) and database searching with the results, and Western blotting for protein identity verification.

In order to separate two samples on the same gel, a new technique known as difference gel electrophoresis (DiGE) was employed instead of traditional 2D gel electrophoresis (Figure 4) [39]. The primary benefit of this technique is that the gel-to-gel variation arising in actual operation can be avoided. Two electrophilic fluorescent cyanine dyes, PrCy3-*N*-hydroxysuccinimide ester and MeCy5-*N*-hydroxysuccinimide ester (Cy3 and Cy5, respectively), are used to label two different samples. These dyes are of the same molecular weight (Figure 5) and are bound covalently to 1-3% of the available lysine side chains (Figure 6) [40]. This low level of binding does not cause significant alteration of the protein isoelectric points (pIs). This strategy can even be optimized by involvement of a third dye, an electrophilic form of Cy2, with charge and size matched to Cy3 and Cy5, as an internal standard labeled to a third sample [41]. The gel image scanning and sample picking was performed using a custom-built instrument with

a high-resolution cooled Prometrix® CCD camera (CH350 model, 16 bit chip, Photometrics, Munich, Germany) capable of imaging Cy2, Cy3 and Cy5 dyes. The colors and excitation and emission wavelengths of the Cy dyes are shown in Figure 7 and Table 4.

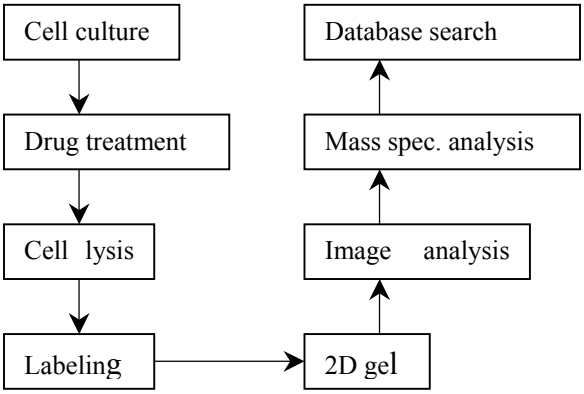

Figure 3: Flow diagram illustrating the overall experimental process in proteomics

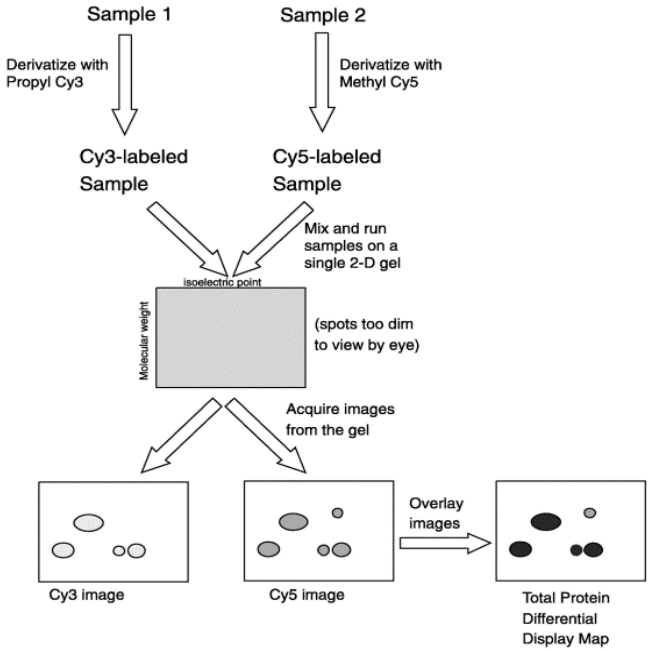

Figure 4: Schematic representation of DIGE [excerpted from Unlu et al., ref. 39]

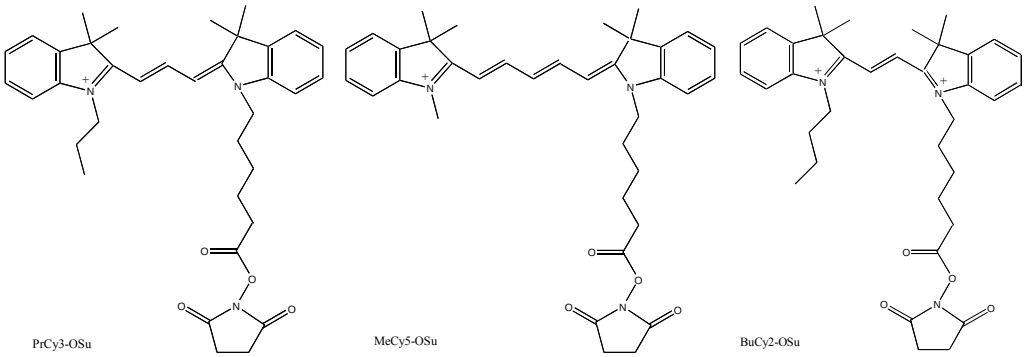

Figure 5: Chemical structures of Cy3 (left), Cy5 (middle) and Cy2 (right)

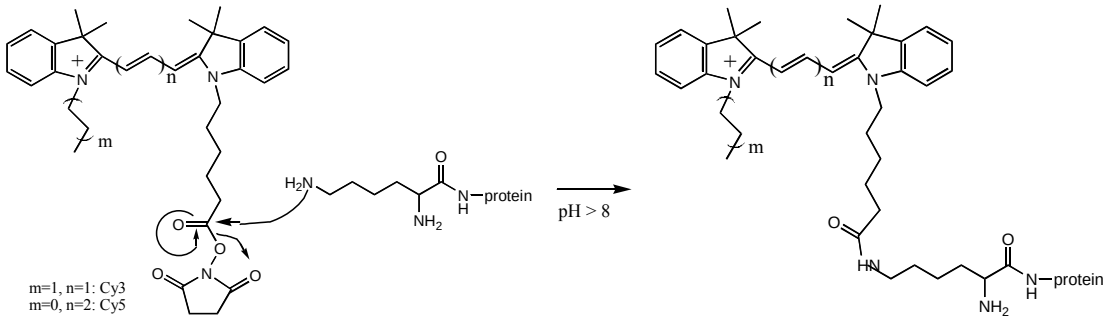

Figure 6: Possible mechanism of Cydye labeling with lysine side chain: an amide is formed through nucleophilic substitution.

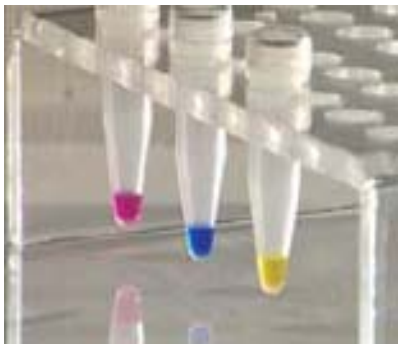

Figure 7: Visual appearances of Cy3, Cy5

Table 4: Parameters of three cyanine dyes

CyDyes	Excitation Wavelength (nm)	Emission wavelength (nm)
Cy2	**489**	**506**
Cy3	**552**	**570**
Cy5	**643**	**667**

By using software accompanying the gel imaging station, two-frame, "flash" movies of the overlying Cy3 and Cy5 images were viewed in a continuous loop to visually detect the differences in the protein patterns between the two samples separated in the same gel. The result was further confirmed and quantified by using DeCyder Differential Analysis software (Amersham Biosciences Inc.). DeCyder analyzes images as fragments, summed to generate a composite image, with proprietary algorithms that detect overlapping, differently colored images within the same gel to match spots and subtract background for normalization. DeCyder creates measurement masks, each outlining an area of the gel containing a protein spot, which were applied to each of the matching fragments in the paired fluorescent images of each gel. The masks define areas in which the pixel values were integrated to create three dimensional topographical maps with peaks representing each protein spot. An estimate of the local background for each spot determined the base values across the masked area. Output from the image analysis, designated as fluorescence intensity, was the sum of pixel values in the mask area minus the background. Volumes of the peaks representing the relative strengths of fluorescent signals from the matched spots were compared [42]. The Melanie 4 viewer (Swiss Institute of Bioinformatics, Switzerland), ImageJ (http://rsb.info.nih.gov/ij/) and V++® Precision

Digital Imaging System (Digital Optics Ltd) are presently being explored in a combined use manner to achieve the best results for image analysis.

2.2.2. Experimental section

2.2.2.1. Materials

Carcinoma cells were from ATCC (American Type Culture Collection), Manassas, VA.

MT stabilizing agents were from our collaborators. Tris-base, glycine, SDS, Coomassie G250 Stain, Tween-20, polyvinylidene difluoride (PVDF) membrane were obtained from Bio-Rad Laboratories, Hercules, CA. 2-Mercaptoethanel, ammonium bicarbonate was from Sigma, St. Louis, MO. Paclitaxel was from NCI Drug Synthesis Branch. ProtoGel 30% (w/v) acrylamide: 0.8 % (w/v) bis-acrylamide stock solution was from National Diagnostics, Atlanta, GA. TGS buffer, MES buffer, MOPS buffer, carrier ampholytes, IPG strips and PROTEAN II gels were from Bio-Rad. ReadyPrep 2D Cleanup Kit, including precipitating agent 1 and 2, wash agent 1 and 2 and wash agent 2 additive, were from Bio-Rad, Hercules, CA. The 2D Quant kit was from Amersham Biosciences, Piscataway, NJ. Cy-dyes were synthesized in Professor Day's lab according to a previously published method [39]. Protease inhibitor cocktail and phosphatase inhibitor cocktail were from EMD Biosciences, Inc., La Jolla, CA. Anti-stathmin antibody (rabbit) was from Santa Cruz Biotechnologies. Peroxidase labeled anti-rabbit antibody (mouse) was from Amersham Life Sciences.

2.2.2.2. Methods

Cell culture and cell lysis Human carcinoma cells were cultured in Dulbecco's modified Eagle's medium (DMEM) supplemented with 10% fetal bovine serum (FBS). Cells were treated with different MT stabilizing agents at their GI90 concentrations for 6 h. After harvest, cells were centrifuged at 1000g and washed with Hank's buffer three times. Cell lysis was performed in 6 M urea, 2 M Thiourea, 100 mM DTT, 4% CHAPS and 10 mM HEPES plus additives (1 mM PMSF, 1.5 mM EDTA, 2 μg/ml aprotinin, 10 μg/ml leupeptin, 1 μg/ml pepstatin-A, 10 mM sodium fluoride and 1 mM sodium orthovanadate). The lysate was ultracentrifuged at 200,000g for 1 h at 4 °C and the supernatant was kept at –80°C for later use.

Acetone protein precipitation The cell lysate protein sample was placed in an acetone-compatible tube followed by adding four volumes of cold acetone (-20°C). The mixture was vortexed and incubated for 2~3 h at -20°C. A subsequent 10 min centrifugation step at 16,000*g* at 4 °C was performed. The supernatant was decanted and properly disposed. The pellet was dried in air and then resuspended in lysis buffer until fully dissolved. The sample was stored at –80°C until ready for use.

Protein sample clean-up (alternative to acetone protein precipitation) The protein sample (100-500 μg) in a final volume of 100 μL was transferred into a 1.5 mL micro-centrifuge tube. Then 300 μL of precipitating agent 1 was added and mixed by vortexing. After incubation on ice for 15 min, 300 μL of precipitating agent 2 was added and the contents mixed by vortexing. The tubes were centrifuged at >12,000*g* for 5 min to form a tight pellet. The supernatant was decanted and the tubes were repositioned as before and centrifuged. Any residual liquid at the bottom of the tubes was removed. Then, 40 μL of wash agent 1 was added on top of the pellet

and the tubes were centrifuged at >12,000*g* for 5 min. The supernatant was removed and discarded. Ultrapure water (25 μL) was added to the tubes and the contents mixed by vortexing 10~20 sec. An additional 1 mL of wash agent 2 (pre-chilled at –20°C for > 1 h) and 5 μL of wash 2 additive were mixed by vortexing for 1 min. During the following incubation period (at –20°C for 30 min), the tubes were vortexed for 30 sec at every 10 min interval. The pellet was formed by centrifugation at >12,000*g* for 5 min. The supernatant was discarded and the pellet air dried for < 5 min (The pellet became translucent once sufficiently dry). The pellet was resuspended by adding lysis buffer followed by vortexing for 1 min, incubation at room temperature for 3~5 min and vortexing again for 1 min. The tubes were centrifuged at >12,000*g* for 2~5 min to clarify the protein sample. The supernatant was then ready for isoelectric focusing (IEF). The remaining sample was stored at –80°C for later use.

Protein quantitation assay

1. Bradford Assay (CBB Assay) The protein sample (2 μL) was added to a 1.5 mL Eppendorf tube and treated with 800 μL of H_2O and 200 μL of Coomassie Protein Assay Reagent (stored at 4 °C). The estimated final concentration of the protein in each sample was 1-20 μg/mL. Protein standards were prepared containing a range of 1 to 20 μg protein (albumin or gamma globulin) the same way to a final volume of 1 mL. The mixtures were vortexed briefly. The absorbance of each sample was read at 595 nm on a SpectraMax Plus UV detector (Molecular Devices). The concentration was calculated from the standard calibration curve. Good detection limits were 1-20 μg with a non-linear standard curve [43].

2. 2-D Quant Kit Tubes containing 1~50 μL of each sample were prepared to be assayed in duplicate. The tubes were treated with 500 μL of precipitant solution, vortexed briefly and incubated for 2-3 min at room temperature. Another 500 μL of co-precipitant solution

was added and the contents mixed briefly by vortexing or inversion. The tubes were centrifuged at a minimum of 10,000*g* for 5 min. The supernatant was decanted and the tubes were centrifuged again. Any liquid remaining was then removed. The pellets were treated with 100 μL of copper solution and 400 μL of de-ionized water to dissolve the pellet. Another 1 mL of working color reagent was added and mixed by inversion. The contents were incubated at room temperature for 15-20 min. The absorbance of each sample was read at 480 nm using water as the reference. The concentration of protein was calculated from a standard curve built with bovine serum albumin. The linear response range of the assay was 0.5~50 μg.

Cy-dye labeling

Cy-dye stock solutions (8.6 mM) were prepared in the Day lab by dissolving the solid dyes separately in anhydrous DMF and aliquoting into 10 μL working solutions. The stock solution was stored at –80°C.

Equal amounts of protein samples (lysates from DMSO-treated control vs. drug-treated cells) were placed into four tubes (two for each sample). The final volume in each tube was equalized with lysis buffer. The samples were labeled in a reciprocal manner as shown in Table 5.

Each tube was treated with 1.0 μL of the PrCy3-OSu or 0.44 μL of the MeCy5-OSu DMF solution and incubated on ice in the dark for 20 min. Afterwards, 1.0 μL of a hydroxysuccinide ester-quenching solution (5 M methylamine in 100 mM HEPES, pH 8.0) was added and the samples incubated on ice in the dark for another 30 min. The paired tubes (Cy3 and Cy5 for each gel) were pooled and mixed well. An ampholyte solution (Bio-Lyte 3/10) (2 μL) was added to each tube (final concentration of ampholyte is ~0.2% (v/v)) and the contents were mixed well for rehydration.

Table 5: Principle of reciprocal labeling in 2D-DiGE experiments

	Gel 1	Gel 2
Control	**Cy3**	**Cy5**
Drug-treated sample	**Cy5**	**Cy3**

IEF focusing Each sample (50-100 µg) was prepared in a rehydration buffer (6 M urea, 2 M Thiourea, 2% CHAPS, 25 mM DTT, 0.2% 3~10 Ampholyte [depending on the IPG strip used] and 2 mM glacial acetic acid) to a final volume that was dependent on the method of IPG strip loading, e.g., 120 µL for cuploading of an 11 cm strip; 185 µL for active/passive rehydration of an 11 cm strip; 300 µL for active/passive rehydration of a 17 cm strip. The indicated volume of each sample was pipeted as a line along the back edge of a channel in the IPG focusing tray. The strip was placed with gel side down onto the sample solution and bubbles were removed as much as possible. Each channel was overlaid with mineral oil. The tray was transferred to the cooling platform in PROTEAN IEF cell and isoelectric focusing was initiated with the program shown in Table 6.

2-D gel electrophoresis After first dimension isoelectric focusing, strips were incubated in an equilibration buffer (50 mM Tris, pH 8.6, containing 6 M urea, 30% glycerol and 2% SDS) containing 1% DTT for 15 min, and then incubated in the same buffer containing 4% iodoacetamide (IAA) for another 15 min. The equilibrated strips were placed on 8-16% gradient Tris-HCl polyacrylamide gels, and the separation continued at constant Watts in the running buffer (25mM Tris, pH 8.8, containing 192 mM glycine and 0.1% SDS) following the program shown in Table 7.

Table 6: Isoelectric focusing program a) Passive/Active rehydration for 11 cm IPG strip; b) Passive/Active rehydration for 17 cm IPG strip and c) Cuploading for 11 cm IPG strip.

a)

Method: Linear			
Rehydration: Passive/Active			
Run Temperature: 20°C			
IPG Strip: *p*H 3~10, 11 cm			
Step 1:	250 V	Ramp: R	Time: 00:15
Step 2:	8,000 V	Ramp: L	Time: 02:00
Step 3:	8,000 V	Ramp: R	Vhour: 30,000
Step 4:	500 V	Hold	Time: 99:00
Focusing current: 50 µA/strip			

b)

Method: Linear			
Rehydration: Passive/Active			
Run Temperature: 20°C			
IPG Strip: *p*H 3~10, 17 cm			
Step 1:	250 V	Ramp: R	Time: 00:15
Step 2:	10,000 V	Ramp: L	Time: 03:00
Step 3:	10,000 V	Ramp: R	Vhour: 60,000
Step 4:	500 V	Hold	Time: 99:00
Focusing current: 50 µA/strip			

c)

Method: Linear			
Rehydration: Cuploading			
Run Temperature: 20°C			
IPG Strip: *p*H 3~10, 11 cm			
Step 1:	250 V	Ramp: R	Time: 00:30
Step 2:	8,000 V	Ramp: L	Time: 04:00
Step 3:	8,000 V	Ramp: R	Vhour: 40,000
Step 4:	500 V	Hold	Time: 99:00
Focusing current: 50 µA/strip			

Table 7: Constant Watt program set in second dimension gel electrophoresis.

Step 1:	2 W/gel	Time: 30 min
Step 2:	5 W/gel	Time: 30 min
Step 3:	10 W/gel	Time: 30 min
Step 4:	20 W/gel	Time: 30 min

Protein visualization and image analysis The gels were fixed overnight in water containing 40% v/v methanol and 5% v/v acetic acid. The gel image scanning and sample picking was performed using a custom-built instrument with a high-resolution cooled Prometrix® CCD camera capable of imaging Cy2, Cy3 and Cy5 dyes. DeCyder Differential Analysis software ("DIA" from Amersham Biosciences Inc.) was used to normalize and analyze the digitalized gel images. To confirm the analysis results obtained with DIA, the gels were further stained in SyproRuby staining solution overnight to achieve the maximal linear response of the signal. The gels were then washed in water containing 10% v/v methanol and 7% v/v acetic acid twice (1 h for each wash) followed by gel scanning.

SDS-PAGE and immunoblot analysis Protein samples were incubated in SDS sample buffer (60 mM Tris, pH 6.8, containing 2% SDS, 10% glycerol, 5% β-mercaptoethanol and 0.5% bromophenol blue) at 95 ºC for 5 min and then segregated by SDS-PAGE using the method of Laemmli [44]. The resolved proteins were transferred onto PVDF membranes using a Bio-Rad Trans-Blot Semi-Dry transfer system at 15 V for 60 min in transfer buffer (25 mM Tris containing 19 mM glycine and 20% v/v methanol). After washing in wash buffer (50 mM Tris, pH 7.4, containing 0.5 M NaCl and 0.1% v/v Tween 20), the blots were blocked with 5% (w/v) nonfat dry milk (blocking agent) in washing buffer. The blots were incubated at 4 ºC overnight with polyclonal rabbit anti-stathmin antibody at 1:20,000 dilution, followed by secondary reaction with horseradish peroxidase-conjugated anti-rabbit antibody at 1:50,000 dilution for 1 h. The Amersham ECL chemiluminescence system and Fuji film were used to detect the protein bands. The density changes of bands could be measured using ImageJ software or a densitometer.

2.2.3. Results and discussion

In the first experiment, the H460 NSCLC cell line was treated with the MT stabilizing agent paclitaxel (50 nM, 1 × GI_{90} value) or with vehicle (DMSO) for 6 h. Cell lysates were prepared and the protein samples were purified and labeled in a reciprocal manner with PrCy3-OSu and MeCy5-OSu as outlined above. Aliquots of each sample (control and drug-treated, 50 μg of each) were pooled and resolved in a 11 cm, pH 3-10 NL IPG strip followed by a second dimensional separation on a Bis-Tris gel. DeCyder software was used to detect the sample-dependent differences in protein distribution. Four values of threshold of volume ratio were examined (2.0, 1.5, 1.2 and 1.0 fold) to screen for differences. Dust and artifacts were detected as peaks with slope values of less than one or as clusters of sharp spikes. The results of image analysis showed that there was no detectable proteomic change (volume ratio > 1.2 fold), either expressional or post-translational (e.g., phosphorylation). The possible reasons for this lack of difference in the proteomes might be as follows. First, the treating time was short and hence there was no significant proteomic change induced. Second, the gel used for protein segregation was too small in dimensions to separate proteins as well as needed to detect differences. The expression level changes in the low abundant protein could be hidden by the overlapping high abundant proteins. Third, the amount of protein loaded onto the gel was perhaps insufficient to detect small changes. Therefore, the low abundant proteins were not detected. Fourth, the protein sample was perhaps not purified enough. Some contaminant or unexpected ingredient existing in the whole cell lysate might affect IEF focusing and further the second dimensional protein pattern.

Two approaches could solve the first problem. One would be to extend the drug treatment time; another would be to replace paclitaxel with a different MT stabilizing agent that causes a

faster response in the same cell line. Obviously, the latter is a better solution, as it would not alter the original objective of the project, which is to search for a cell-based, early stage screening method for MT stabilizers. Referring back to the data shown in Table 1, it was therefore decided to employ discodermolide as the test agent. Two parallel experiments were performed based on the treatment of H460 human non-small cell lung carcinoma cells with 1 x GI_{90} and 2 x GI_{90} concentrations of discodermolide. IPG strips of 17 cm length and pH 3-10 (nonlinear, "NL") range were employed to pursue a better first-dimensional focusing and 183 x 193 x 1 mm PROTEAN II gels (8-16% gradient) were used for optimal second-dimensional separation. After electrophoresis, the gels were scanned and two pairs (control and drug-treated labeled each with Cy3 and Cy5 for each concentration) of digitized images were analyzed with DeCyder software. More than 2000 spots were detected for each gel image. The spot intensities were normalized first by subtraction of the local estimates of background and then by adjustment of signals to compensate for dye-specific system gain. A conservative exclusion filter was subsequently applied to reject spots caused by dust particles [45]. Finally, two spots with mid-level changes in expression were detected for each pair (Cy3 and Cy5 labeled) of gel images. The two spots on the image of 1 x GI_{90} concentration were further confirmed to be identical to the two spots on the image of 2 x GI90 concentration based on protein distribution pattern, molecular weight and pI value (Figure 8-12). Table 8 shows the values of the volume ratio changes of the two spots. Since the control (DMSO treated) and the sample (drug treated) were labeled by Cy3 and Cy5 in a reciprocal manner, a pair of increasing and decreasing volume ratio change values must be seen in order for the hypothesis that changes in expression to be accepted. Otherwise, a pair of values with the same sign could be from preferential labeling of one of the two cyanine dyes, meaning ununiformity of labeling.

Table 8: DeCyder DIA image analysis results on reciprocal labeled gels from H460 cells treated with discodermolide.

Gel images	*Spot Index*	*Cy3*	*Cy5*	*Volume ratio changes*
101404_D300_DM	A2	D300	DMSO	- 1.59
101404_DM_D300	A2	DMSO	D300	+1.37
101404_D600_DM	A2	D600	DMSO	- 1.71
101404_DM_D600	A2	DMSO	D600	+1.67
101404_D300_DM	A1	D300	DMSO	+1.68
101404_DM_D300	A1	DMSO	D300	- 1.04
101404_D600_DM	A1	D600	DMSO	+1.62
101404_DM_D600	A1	DMSO	D600	- 1.56

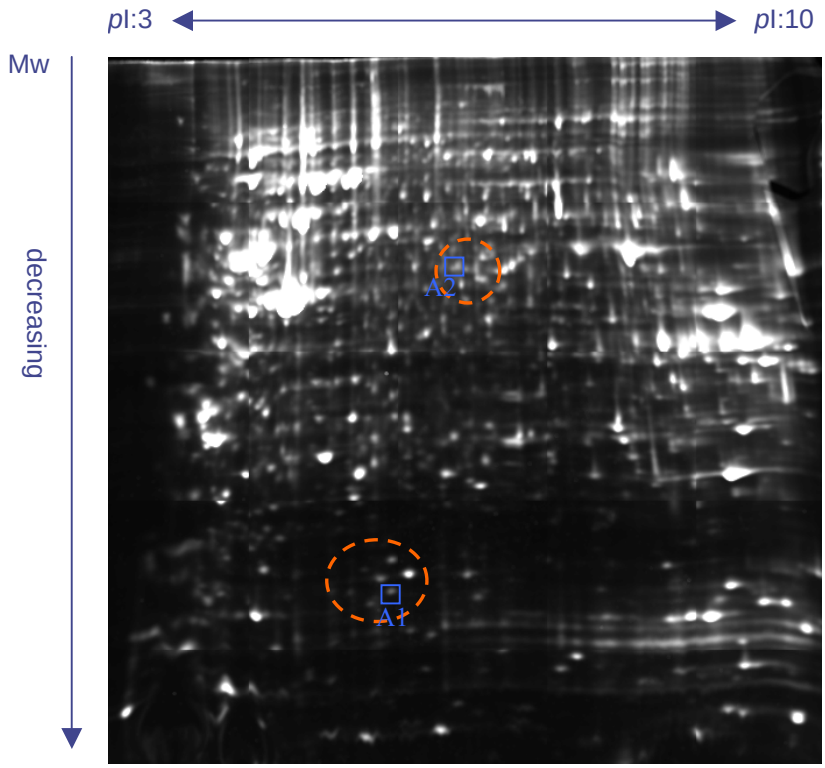

Figure 8: SyproRuby stained gel image acquired after electrophoresis of whole cell lysate of H460 cell line treated with discodermolide. The blue squares encompass two spots detected to have expression changes. The orange dashed circles cover the around area showing the specific pattern in which phosphorylated isoforms might exist.

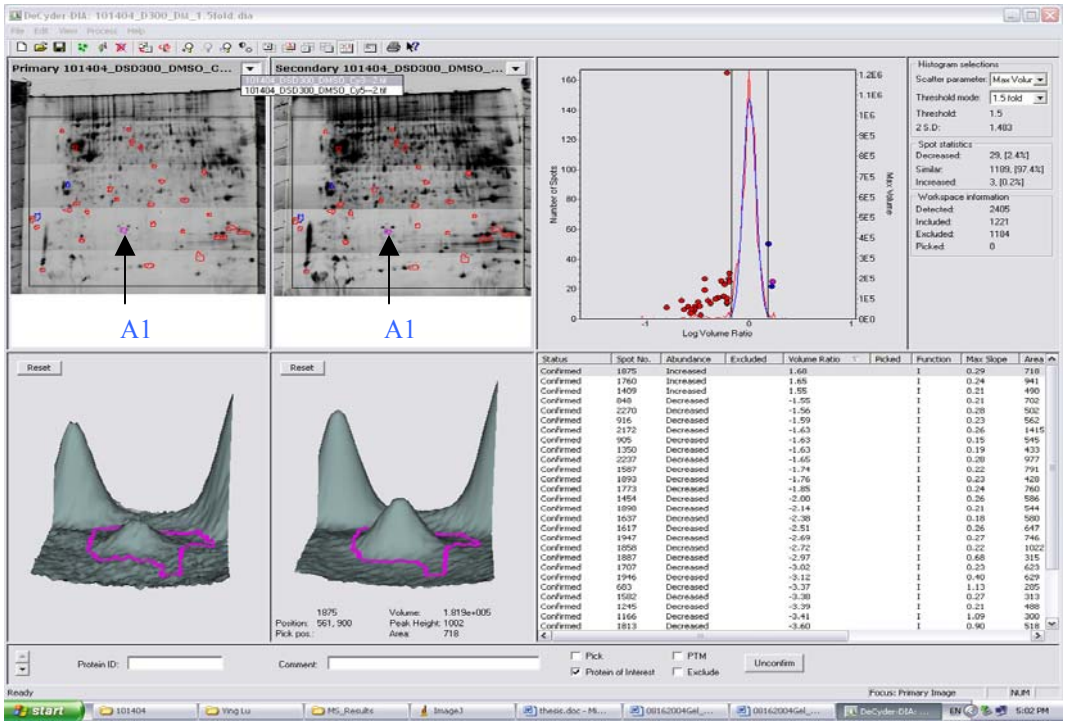

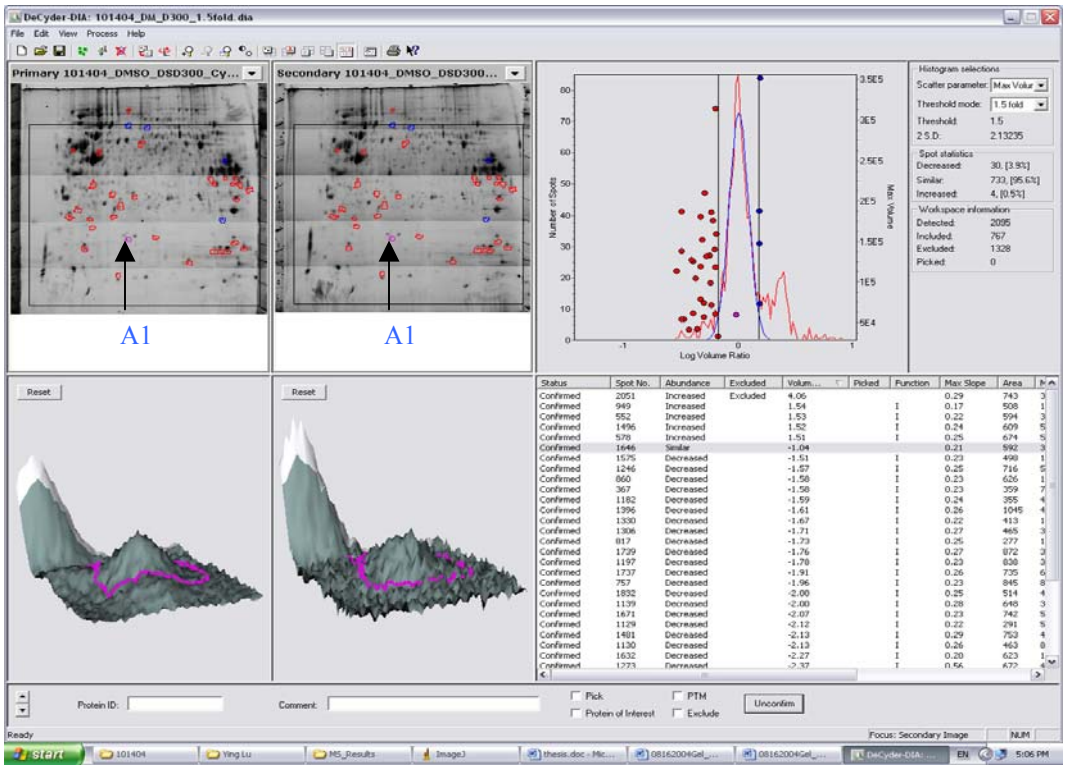

Figure 9: Output of image analysis with DeCyder on gels from DMSO- and discodermolide-treated H460 cell lysates reciprocally labeled with PrCy3-OSu and MeCy5-OSu at 1 × GI90 concentration, showing the position of spot A1 and its 3-D topographical map.

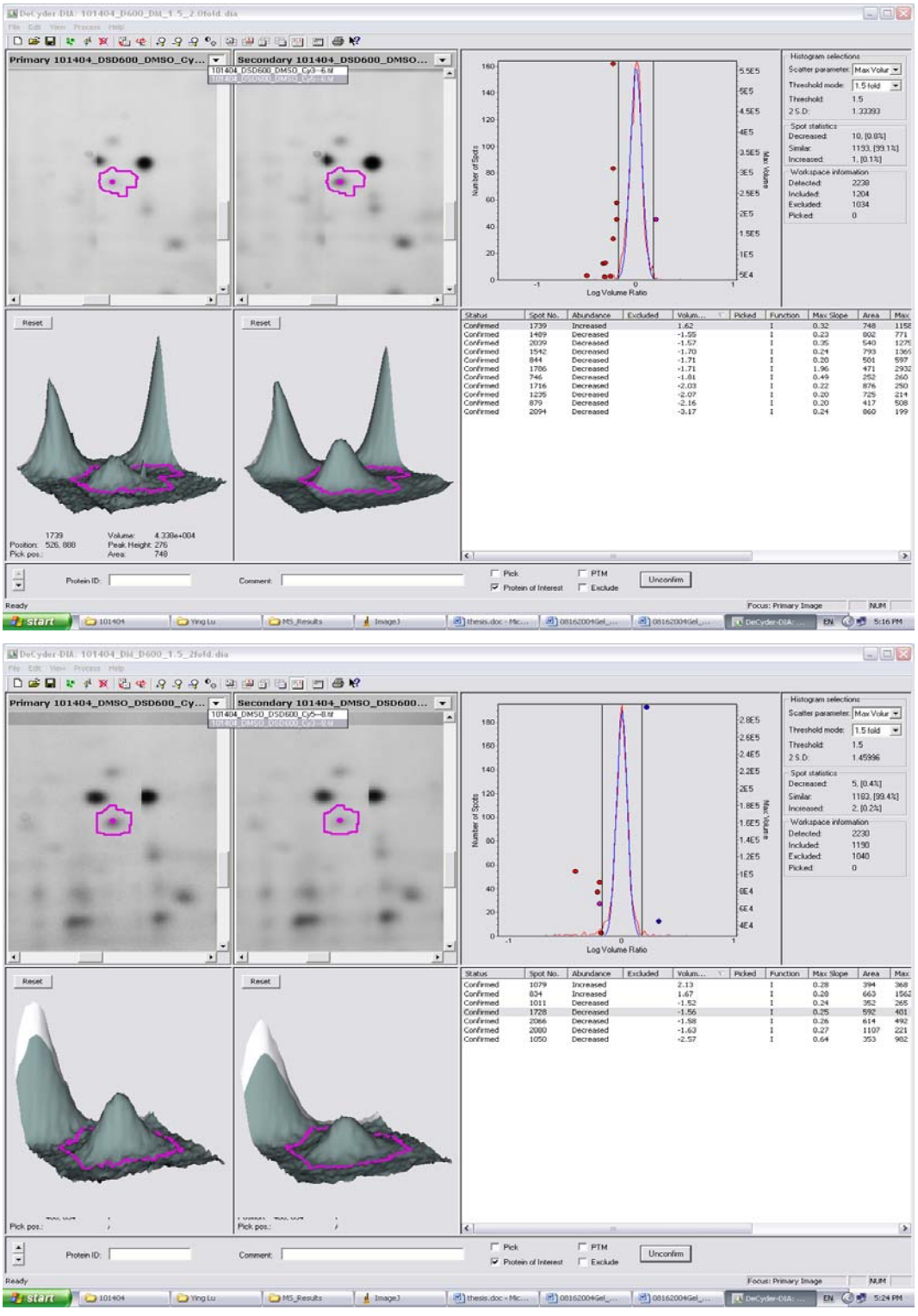

Figure 10: Output of image analysis with DeCyder on gels from DMSO- and discodermolide-treated H460 cell lysates reciprocally labeled with PrCy3-OSu and MeCy5-OSu at 2 × GI90 concentration, showing a zoom-in of the position of spot A1 and its 3-D topographical map.

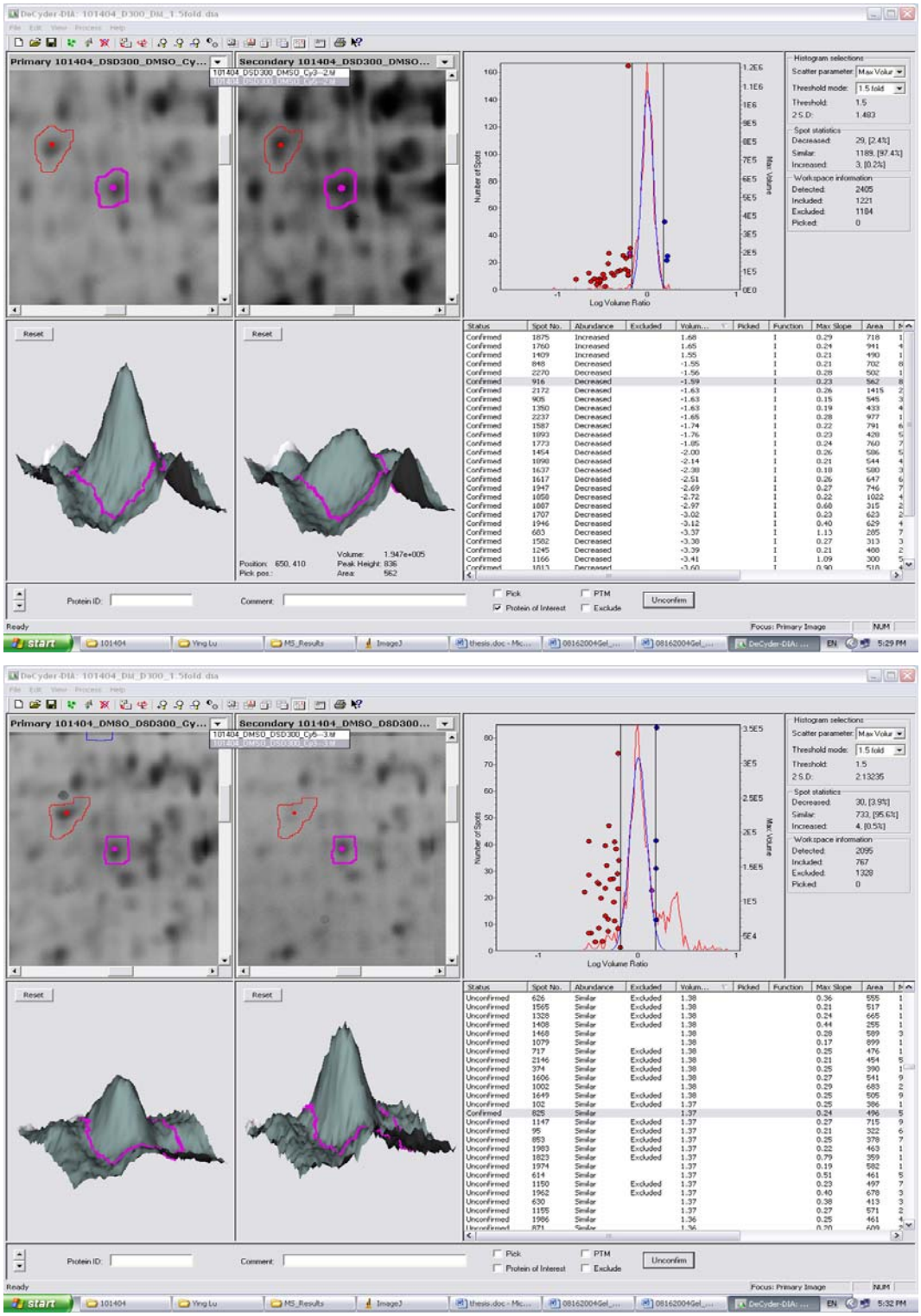

Figure 11: Output of image analysis with DeCyder of gels from DMSO- and discodermolide-treated H460 cell lysates reciprocally labeled with PrCy3-OSu and MeCy5-OSu at 1 × GI90 concentration, showing the zoom-in of the position of spot A2 and its 3-D topographical map.

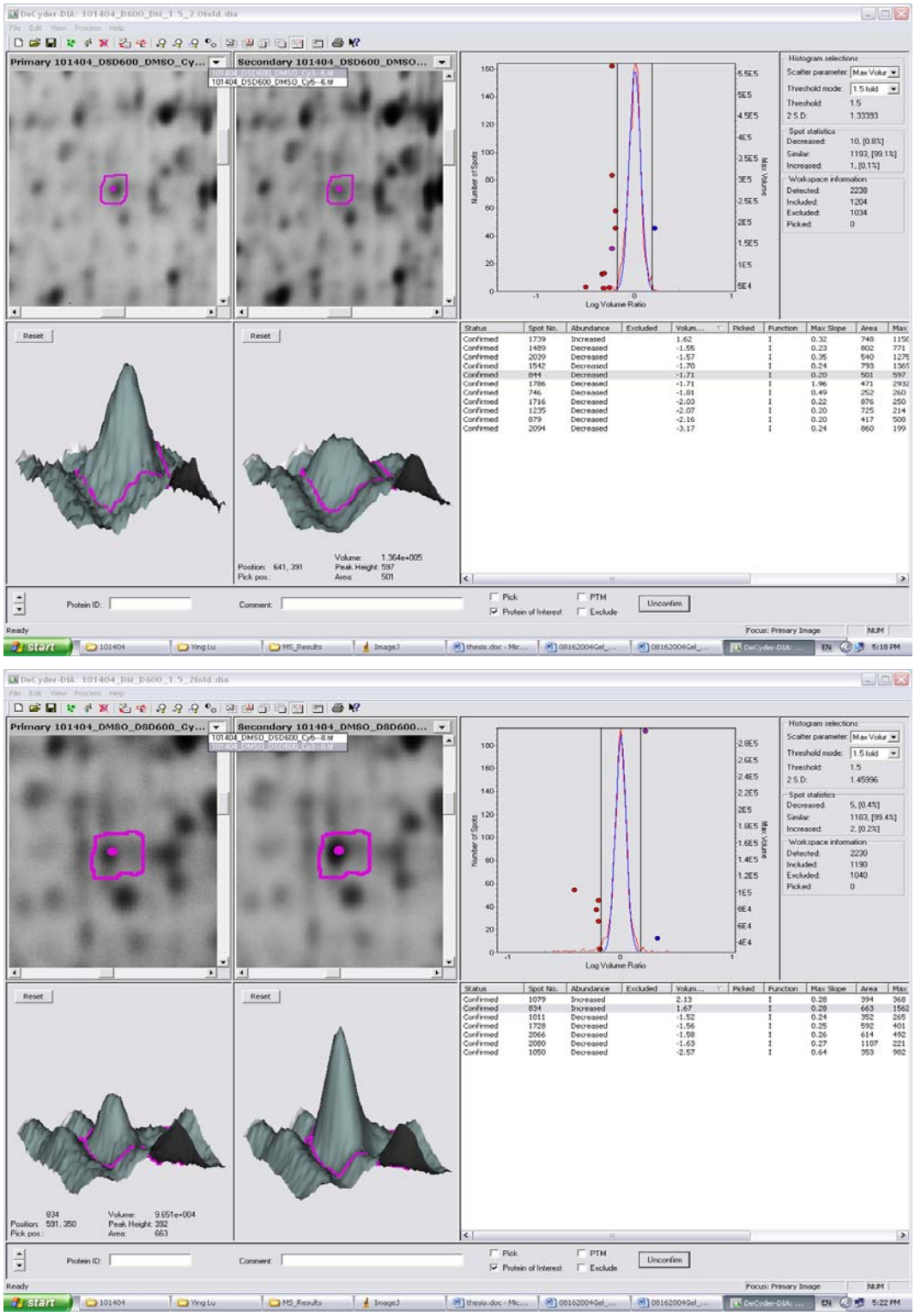

Figure 12: Output of image analysis with DeCyder on gels from DMSO- and discodermolide-treated H460 cell lysates reciprocally labeled by PrCy3-OSu and MeCy5-OSu at 2 × GI90 concentration, showing the zoom-in of the position of spot A2 and its 3-D topographical map.

2.3. PROTEIN IDENTIFICATION BY MASS SPECTROMETRY

2.3.1. Introduction

Mass spectrometry has developed into a powerful tool to analyze proteins for information such as the protein sequence, some three dimensional structure information, as well as any post-translation modifications of the protein[46-48]. With the matrix-assisted laser desorption ionization (MALDI) method, nonvolatile molecules can be readily introduced into the gas phase and analyzed by mass spectrometry. The MALDI sample consists of a solid mixture of analyte mixed with a crystalline matrix on a sample plate. The mixture is excited by laser light resulting in ions that are guided by optics through a mass analyzer and into an ion detector (Figure 13). The matrix is an organic acid with a chromophore absorbing at the laser wavelength, such as α-cyano-4-hydroxycinnamic acid (Figure 14). Generally, the low mass region of such spectra, below ~500 Da, is obscured by the presence of signals from matrix cluster ions.

Enzymatic digestion has been employed extensively as a standard method in proteomic analysis. Typical enzymatic or chemical cleavage methods are listed in Table 9. An enzyme of low specificity, which digests proteins to a mixture of free amino acids and di- and tri- peptides (e.g., Pronase E), is not a good choice. A complex mixture containing large numbers of components of similar mass will result in a complex spectrum consisting of overlapping ion signals. In practice, it is best to use enzymes of specificity equal to or greater than trypsin. Trypsin hydrolyzes polypeptides on the carboxyl side of arginine and lysine residues. In-gel digestion of polyacrylamide gel electrophoresis (PAGE) separated proteins has proved to be an efficient method to generate peptide fragment mixtures for mass spectrometric analyses. Based on the peptide mass fingerprint (PMF) information and if a tandem MS system is available, the

peptide fragments can be selected as precursors for further fragmentation. A series of fragment ions are produced, within which the ***y*** type and ***b*** type ions (Figure 15) are predominant. The database is then searched based on the PMF data combined with MS/MS sequence information.

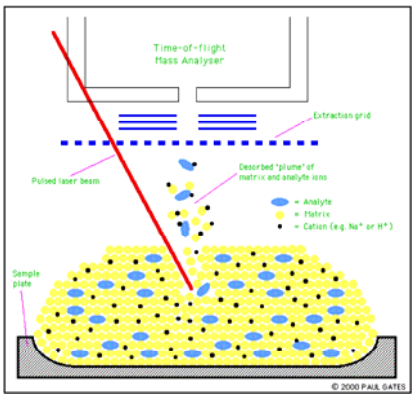

Figure 13: Illustration of MALDI

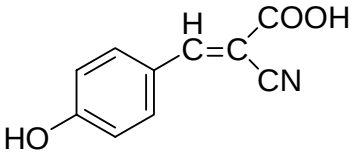

Figure 14: The chemical structure of the matrix molecule: α-cyano-4-hydroxycinnamic acid (CHCA)

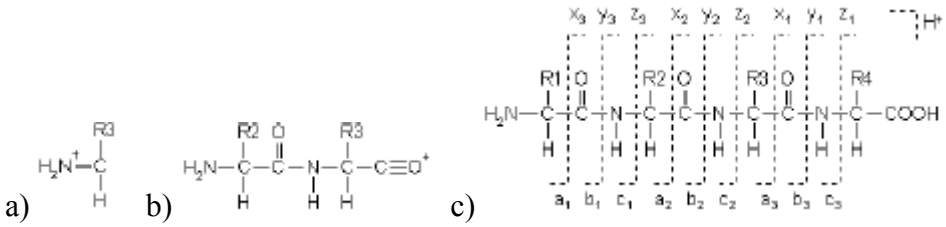

Figure 15: A generic example showing a) an immonium ion, b) an internal ion and c) x, y, z, a, b, and c ion series.

Table 9: Typical enzymatic and chemical cleavage methods used in proteomics.

Name	Site of Cleavage	Will not cleave after	N or C terminal
Typsin	K, R	P	C term
Arg-C	R	P	C term
Asp-N	B, D		N term
Asp-N_ambic	D, E		N term
Chymotrypsin	F, Y, W, L, I, V, M	P	C term
CNBr	M		C term
Formic_acid	D		C term
Lys-C	K	P	C term
Lys-C/P	K		C term
PepsinA	F, L		C term
Tryp-CNBr	K, R, M	P	C term
TrypChymo	F, Y, W, L, K, R	P	C term
Trypsin/P	K, R		C term
V8-DE	B, D, E, Z	P	C term
V8-E	E, Z	P	C term
CNBr + Trypsin	M		C term
	K, R	P	C term

2.3.2. Experimental section

2.3.2.1. Materials

Both sequencing grade and Gold grade trypsin were from Promega, Madison, WI. CHCA matrix was from Sigma and recrystallized in the Day lab. Ammonium bicarbonate and formic acid were obtained from Sigma, St. Louis MO. Acetonitrile and methanol were obtained from Fisher, Fairlawn, NJ.

2.3.2.2. Methods

In gel tryptic digestion After staining the 1-D SDS-PAGE gels with Coomassie blue, the bands of interest were excised and soaked in 1:1 (v/v) methanol-50mM aq. NH_4HCO_3 for 30 min with shaking for full destaining. The supernatant was removed and the destaining process was repeated one more time. Then the gel pieces were treated with 100% acetonitrile for 5-10 min. Enough aq. 10 mM DTT/25 mM NH_4HCO_3 was added to cover each individual gel piece and the mixtures were incubated at 56 ºC for 1 h with shaking for reduction of any disulfide bonds. The supernatant was removed and 50 mM iodoacetamide/25mM NH_4HCO_3 was added for alkylation of cystein sulfhydryls (thiol, -SH) followed by incubation in the dark for 45 min at room temperature. The supernatant was removed and 25 mM NH_4HCO_3 was added. After 10 min of vortex mixing, the supernatant was removed and the gel plugs were soaked in 1:1 (v/v) CH_3CN-25mM aq. NH_4HCO_3 for 5 min with vortex mixing. The same process was repeated and then the gel pieces were completely dried in a Speed-Vac. For gel pieces excised from 2-D gels, reduction and alkylation was not performed. After these gel pieces were washed with 1:1 (v/v) methanol-50 mM aq. NH_4HCO_3 two times, 100% acetonitrile was added with 5-10 min of shaking and then the pieces were dried in a Speed-Vac. The dried gel pieces were kept at -4 ºC until ready for tryptic digestion.

Tryptic digestion was performed via the addition of 10 μL of trypsin (20 ng/μL) in 25 mM aqueous ammonium bicarbonate and incubation at ambient for 10-15 min for full rehydration, followed by incubation at 42 ºC for 4 h with agitation. The trypsin solution in each tube was then transferred to a new clean tube. The remaining gel pieces were treated with 60 μL of 1% TFA in 50% aqueous acetonitrile for 30 min two times. The extracts of each treatment were pooled with the trypsin solution and the mixtures were dried in a Speed-Vac.

Mass spectrometric analysis A saturated solution of CHCA was prepared in 0.3% TFA in 50% aqueous acetonitrile containing 1 mM ammonium citrate. Recovered peptides were resuspended in 3 μL of 0.3% TFA in 50% aqueous acetonitrile containing 1 mM ammonium citrate and then diluted with the saturated CHCA solution. Samples (0.7 μL) were spotted onto the stainless steel MALDI plate and allowed to dry. Masses of peptides were determined using an Applied Biosystems 4700 MALDI-TOF-MS (Applied Biosystem, MA). Internal calibration was performed using trypsin autolysis signals (*m/z* 842.51 and 2211.10). Peptide sequences were determined using MALDI-TOF/TOF-MS/MS with 1 kV fragmentation with ambient air as the collision gas and spectra were externally calibrated with an MS/MS spectrum from the *m/z* 1570.68 $[M+H]^+$ ion (Glu^1-Fibrinopeptide B). Database searching was performed using GPS Explorer software (Applied Biosystems, MA) or using online search engines, e.g., Mascot (http://www.matrixscience.com/search_form_select.html),

MS-Fit (http://prospector.ucsf.edu/ucsfhtml4.0/msfit.htm),

or Profound (http://prowl.rockefeller.edu/profound_bin/WebProFound.exe).

2.3.3. Results and discussion

The protein identification was performed based on the combined PMF and peptide sequence information acquired from MALDI-TOF experiments. The results showed that two spots, A1 and A2 (Figure 8.), were the proteins stathmin and eukaryotic elongation factor 1 gamma (EEF1G), respectively (Figure 16-17, Table 10-14).

Stathmin is a well conserved and highly expressed protein in proliferating cells and neurons. Its expression level changes markedly during development, cellular differentiation and tissue regeneration, and is elevated in some neoplastic cells [49]. Depending on its phosphorylation

status, stathmin either inhibits microtubule polymerization or destalibizes microtubules by sequestering free tubulin heterodimers. The destabilization activity occurs in the non-phosphorylated form. Phosphorylation occurs at four serines of stathmin, residues 16, 25, 38 and 63 [50]. These four phosphorylation sites are targets of multiple kinases, e.g., mitogen-activated protein (MAP) kinase for Ser25, cyclin-dependent kinases (Cdks) for both Ser25 and Ser 38, protein kinase A (PKA) for Ser16 and Ser63, and Ca^{2+}/calmodulin-dependent kinase-Gr (CaMK IV/Gr) for Ser16 [49]. Although there are various phophorylation combinations, it appears that phosphorylaion at Ser16 and Ser63 inhibits stathmin to a greater extent than phosphorylations at Ser25 and Ser38 [51-53]. Figure 18 illustrates the phosphorylation mediated regulation of stathmin activity during cell cycle progression [54]. In the present experiments, the expression level of stathmin was found to be decreased in discodermolide-treated cells with respect to their DMSO-treated control. The reason might be that discodermolide stabilizes the microtubules and leads to a decrease in concentration of free tubulin. Consequently, the low level of tubulin concentration could result in decreased expression of stathmin.

Eukaryotic elongation factors (EEF) include both EEF1 and EEF2. EEF1 consists of two different subfactors: EEF1A and EEF1B. EEF1A (formerly eEF1α) is a single polypeptide while EEF1B is a multitrimer of EEF1Bα (formerly eEF1β), EEF1Bβ (formerly eEF1δ) and EEF1Bγ (formerly eEF1γ) polypeptides. In general, the process of protein elongation is composed of two steps, the recruitment of amino-acylated tRNA to an existing ribosome/mRNA complex and the translocation of the ribosome along the mRNA as amino acids are added to the protein. EEF1A and EEF1B regulate the recruitment and EEF2 controls the translocation. As shown in Figure 19, one EEF1B complex can associate with two EEF1A proteins. The EEF1B consists of either one molecule of each of EEF1Bα and EEF1Bβ or two molecules of EEF1Bα, or two molecules of

EEF1Bβ. Both EEF1Bα and EEF1Bβ function to exchange GTP for GDP on EEF1A, and EEF1Bγ has no known enzymatic activity but facilitates the physical association of EEF1Bα or EEF1Bβ with each other or with EEF1A [55].

Furthermore, EEF1A, has also been reported to be a microtubule-servering factor [56]. Its microtubule-servering activity can be inhibited by the addition of free tubulin or of the microtubule-associated proteins p220 [57] or MAP2 [58]. Because microtubule reorganization occurs during the transition from interphase to mitosis, an unregulated elevated level of expression of EEF1A might be related with cell death [59]. However, some other reports found that both EEF1A1 and EEF1A2 inhibit apoptosis [60-62]. The present data showed an increased level of EEF1Bγ in the drug-treated sample compared to the DMSO-treated control. A possible explanation of this phenomenon might be that the carcinoma cells are attempting to elevate the expression level of EEF1A as a response against the apoptosis inducing actions of discodermolide, a microtubule stabilizing agent. Accordingly, EEF1Bγ might also be over-expressed because it serves to couple EEF1Bα and EEF1Bβ to EEF1A and therefore activate EEF1A's GTP exchanging activity.

Besides spots A1 and A2, other spots without detectable expression changes were also identified for protein cataloguing purposes. Table 15 and 16 list the results based on experiments where samples (discodermolide-treated cells vs. DMSO-treated control) were segregated on different sized gels (Figure 20, 21).

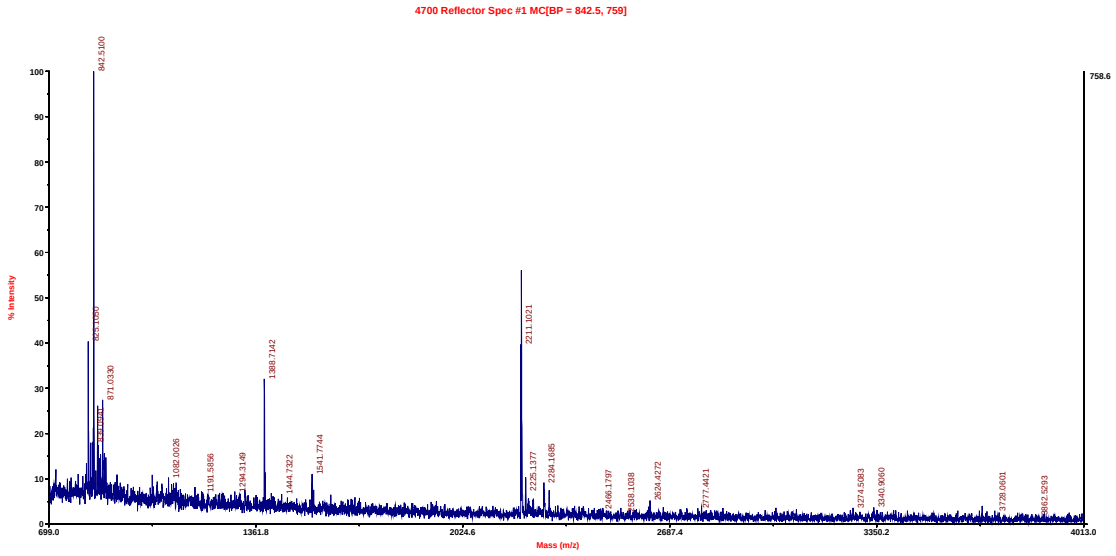

Figure 16: MALDI mass spectrum of spot A1

Table 10: Database search result for spot A1. Red bold text represents the matched peptide sequence within the complete sequence of stathmin. Sequence coverage: 18%

Rank	Protein Name	Accession Number	Protein MW	Protein PI	Peptide Count	Protein Score	Protein Score C.I. %	Total Ion Score	Total Ion Score C.I. %	Best Ion Score	Best Ion Score C.I. %
1	Stathmin 1 [Homo sapiens]	gi|15680064	17325.9	5.76	2	135	100	120	100	77	100

Peptide Number	Calculated Mass	Observed Mass	Match Error Da	Match Error PPM	Start Position	End Position	Sequence	Ion Score	Ion Score C.I. %	Modification
1	1388.7532	1388.7638	0.0106	8	15	27	ASGQAFELILSPR	77	100	
2	1541.8209	1541.826	0.0051	3	28	41	SKESVPEFPLSPPK	42	99.9	

1 MASSDIQVKE LEKR**ASGQAF ELILSPRSKE SVPEFPLSPP K**KKDLSLEEI
51 QKKLEAAEER RKSHEAEVLK QLAEKREHEK EVLQKAIEEN NNFSKMAEEK
101 LTHKMEANKE NREAQMAAKL ERLREKDKHI EEVRKNKESK DPADETEAD

Table 11: Comparison of theoretical fragment ions of the precursor *m/z* 1388.76 $[M+H]^+$ ion with observed MS/MS ions. Red bold text represents the matched ions.

#	Immon.	a	a*	a^0	b	b*	b^0	Seq	v	v*	v^0	#
1	44.05	44.05			72.04			A				1
2	60.04	131.08		113.07	159.08		141.07	S	1317.72	1300.69	1299.71	1
3	30.03	188.10		170.09	216.10		198.09	G	1230.68	1213.66	1212.67	1
4	101.07	316.16	299.14	298.15	**344.16**	327.13	326.15	O	1173.66	1156.64	1155.65	1
5	44.05	387.20	370.17	369.19	**415.19**	398.17	397.18	A	**1045.60**	1028.58	1027.59	9
6	120.08	534.27	517.24	516.26	**562.26**	545.24	544.25	F	974.57	957.54	956.56	8
7	102.06	663.31	646.28	645.30	**691.31**	674.28	673.29	E	**827.50**	810.47	809.49	7
8	86.10	776.39	759.37	758.38	**804.39**	787.36	786.38	L	**698.46**	681.43	680.45	6
9	86.10	889.48	872.45	871.47	**917.47**	900.45	899.46	I	**585.37**	568.35	567.36	5
1	86.10	1002.56	985.54	984.55	**1030.56**	1013.53	1012.55	L	**472.29**	455.26	454.28	4
1	60.04	1089.59	1072.57	1071.58	1117.59	1100.56	1099.58	S	**359.20**	342.18	341.19	3
1	70.07	1186.65	1169.62	1168.64	**1214.64**	1197.62	1196.63	P	**272.17**	**255.15**		2
1	**129.11**							R	175.12	158.09		1

Observed mass (S/N ratio > 10, increasing mass)

754.5472 1188.8651 675.2676 **827.4981** **1030.5472** 316.1245 564.3383 **1214.8143** 277.1194 341.1815
803.3835 141.088 455.2275 390.4466 227.1389 404.1798 212.1358 219.1067 **585.3499** 425.2565
787.3649 733.3005 **1045.6155** 175.1176 461.2084 342.1627 **344.1561** **562.2508** 390.1839 785.4595
917.4638 **129.1074** **415.1925** **691.2664** 112.0851 **472.2663** **255.1333** **804.4049** **359.1846** **698.4545**
272.162

Table 12: Comparison of theoretical fragmentation of the precursor *m/z* 1541.83 $[M+H]^+$ ion with observed MS/MS values. Red bold text represents the matched ions.

#	Immon.	a	a*	a^0	b	b*	b^0	Seq	v	v*	v^0	#
1	60.04	60.04		42.03	88.04		70.03	S				1
2	101.11	188.14	171.11	170.13	**216.13**	199.11	198.12	K	1454.79	1437.76	1436.78	1
3	102.06	317.18	300.16	299.17	345.18	328.15	327.17	E	1326.69	1309.67	1308.68	1
4	60.04	404.21	387.19	386.20	432.21	415.18	414.20	S	1197.65	1180.63	1179.64	1
5	72.08	503.28	486.26	485.27	**531.28**	514.25	513.27	V	1110.62	1093.59	1092.61	1
6	70.07	600.34	583.31	582.33	628.33	611.30	610.32	P	**1011.55**	994.52	993.54	9
7	102.06	729.38	712.35	711.37	757.37	740.35	739.36	E	914.50	897.47	896.49	8
8	120.08	876.45	859.42	858.44	**904.44**	887.42	886.43	F	**785.46**	768.43	767.45	7
9	70.07	973.50	956.47	955.49	1001.49	984.47	983.48	P	**638.39**	621.36	620.38	6
1	86.10	1086.58	1069.56	1068.57	**1114.58**	1097.55	1096.57	L	541.33	524.31	523.32	5
1	60.04	1173.62	1156.59	1155.60	**1201.61**	1184.58	**1183.60**	S	428.25	411.22	410.24	4
1	70.07	1270.67	1253.64	1252.66	**1298.66**	1281.64	1280.65	P	**341.22**	324.19		3
1	70.07	1367.72	1350.69	1349.71	1395.72	1378.69	1377.71	P	244.17	227.14		2
1	101.11							K	147.11	130.09		1

Seq	ya	yb
PEFPLS	643.35	671.34
EFPLSP	643.35	671.34
PL	183.15	211.14

Observed mass (S/N ratio > 10, increasing)

1478.0942 271.1662 129.1104 **216.1142** 584.334 1497.1174 **1183.5425**
1115.6123 **1298.7189** 1490.1952 1389.7218 1491.801 **211.1322** 84.0837
323.2235 1388.8489 **531.298** **1114.5524** 1544.842 **671.3597** **904.4625**
1541.8344 **785.472** **341.2069** **1201.6334** **638.3813** **1011.5574**

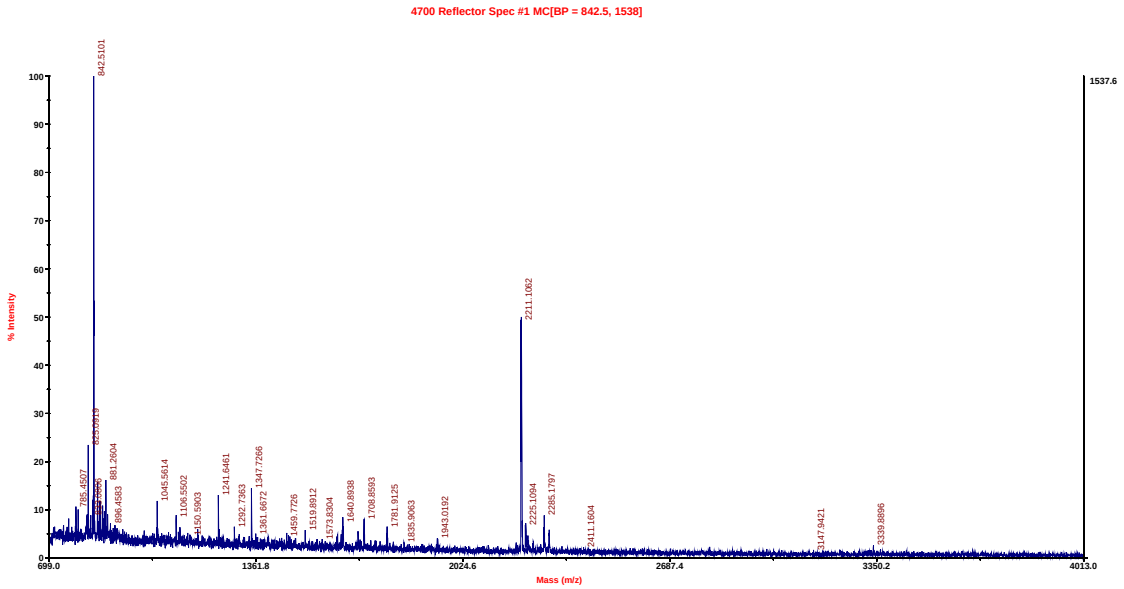

Figure 17: MALDI mass spectrum of spot A2

Table 13: Comparison of theoretical fragmentation of the precursor *m/z* 1241.63 [M+H[$^{+}$ ion with observed MS/MS values. Red bold text represents the matched ions.

#	Immon.	a	a*	a^0	b	b*	b^0	Seq	y	y*	y^0	#
1	60.04	60.04		42.03	**88.04**		70.03	S				1
2	74.06	161.09		143.08	189.09		171.08	T	1154.62	1137.59	1136.61	9
3	120.08	308.16		290.15	**336.16**		318.15	F	1053.57	1036.55	1035.56	8
4	72.08	407.23		389.22	**435.22**		417.21	V	906.50	889.48	888.49	7
5	86.10	520.31		502.30	548.31		530.30	L	807.44	790.41	789.43	6
6	**88.04**	635.34		617.33	663.34		645.32	D	694.35	677.33	676.34	5
7	102.06	764.38		746.37	792.38		774.37	E	**579.33**	562.30	561.31	4
8	120.08	911.45		893.44	939.45		921.44	F	**450.28**	**433.26**		3
9	101.11	1039.55	1022.52	1021.54	1067.54	1050.51	1049.53	K	**303.21**	286.19		2
1	**129.11**							R	**175.12**	158.09		1

Seq	ya	yb
TFVL	**433.28**	461.28

Observed mass (S/N ratio > 10, increasing)

288.2281 **435.2228** 504.2939 1185.3153 **88.0927** 125.2726 681.4937
433.2856 1189.847 581.3318 **336.1622** 1197.9047 **129.0966** **450.303**
303.2187 **579.363** 1241.7217 **175.1171**

Table 14: Database search result of spot A2. Red bold text represents the matched peptide sequence within the complete sequence of EEF1G. Sequence coverage: 18%

Rank	Protein Name	Accession Number	Protein MW	Protein PI	Peptide Count	Protein Score	Protein Score C.I. %	Total Ion Score	Total Ion Score C.I. %	Best Ion Score	Best Ion Score C.I. %
1	EEF1G protein [Homo sapiens]	gi|39644794	49814	6.27	8	62	99.681	27	97.294	27	97.294

Peptide Number	Calculated Mass	Observed Mass	Match Error Da	Match Error PPM	Start Position	End Position	Sequence	Ion Score	Ion Score C.I. %	Modification
1	821.45	821.46	0.0154	19	147	153	TFLVGER			
2	1118.68	1118.67	-0.005	-4	135	144	ILGLLDAYLK			
3	1241.65	1241.63	-0.0192	-15	283	292	STFVLDEFKR	27	97.294	
4	1274.78	1274.76	-0.0173	-14	134	144	RILGLLDAYLK			
5	1347.73	1347.70	-0.0325	-24	15	27	ALIAAQYSGAQVR			
6	1399.66	1399.69	0.0321	23	1	11	GTLYTYPENWR			
7	1684.77	1684.76	-0.0153	-9	412	425	EYFSWEGAFQHVGK			
18	1707.87	1707.85	-0.0184	-11	28	42	VLSAPPHFHFGQTNR			

1 **GTLYTYPENW R**AFK**ALIAAQ YSGAQVRVLS APPHFHFGQT NR**TPEFLRKF
51 PAGKVPAFEG DDGFCVFESN AIAYYVSNEE LRGSTPEAAA QVVQWVSFAD
101 SDIVPPASTW VFPTLGIMHH NKQATENAKE EVR**RILGLLD AYLK**TR**TFLV**
151 **GER**VTLADIT VVCTLLWLYK QVLEPSFRQA FPNTNRWFLT CINQPQFRAV
201 LGEVKLCEKM AQFDAKKFAE TQPKKDTPRK EKGSREEKQK PQAERKEEKK
251 AAAPAPEEEM DECEQALAAE PKAKDPFAHL PK**STFVLDEF KR**KYSNEDTL
301 SVALPYFWEH FDKDGWSLWY SEYRFPEELT QTFMSCNLIT GMFQRLDKLR
351 KNAFASVILF GTNNSSSISG VWVFRGQELA FPLSPDWQVD YESYTWRKLD
401 PGSEETQTLV R**EYFSWEGAF QHVGK**AFNQG KIFK

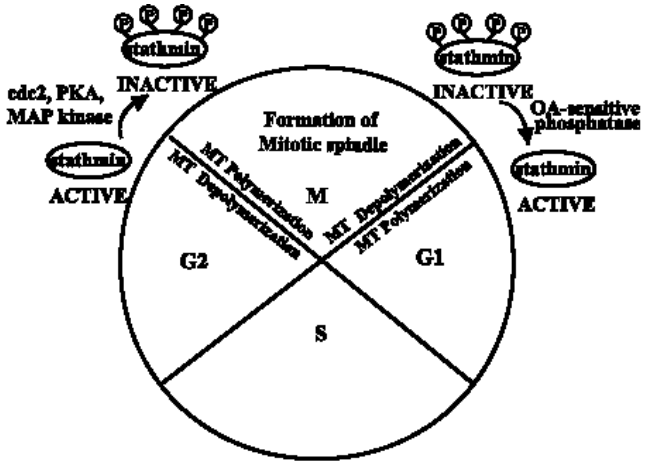

Figure 18: Regulation of stathmin activity during the cell cycle [excerpted from Mistry and Atweh, ref. 54]

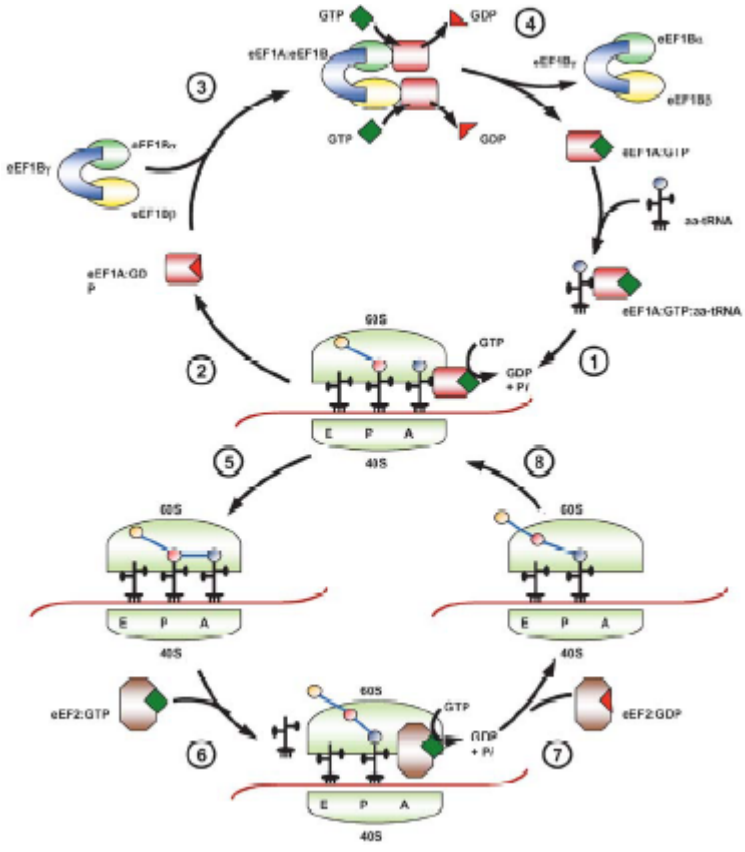

Figure 19: The working phase of the protein elongation process [excerpted from Thornton et al., ref. 55]

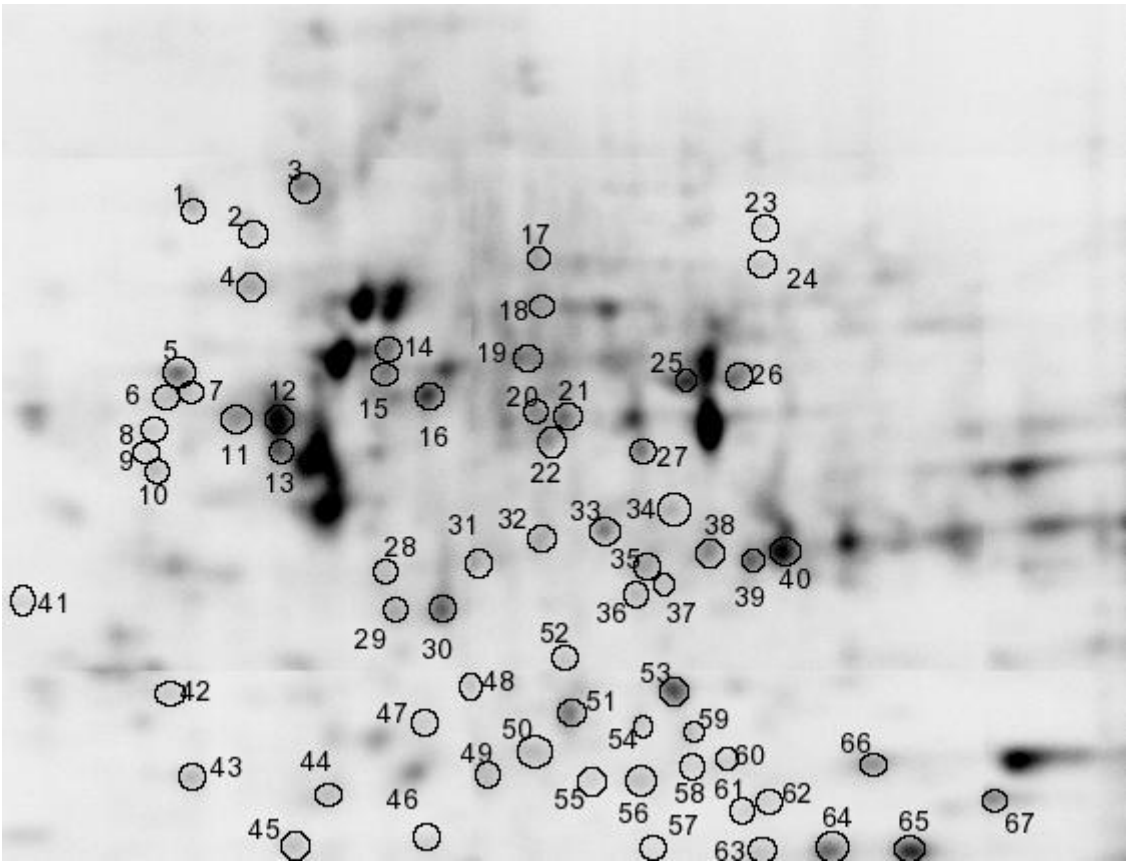

Figure 20: Protein distribution map of discodermolide-treated H460 human non-small cell lung cancer cells after electrophoresis in 11 cm gel

Table 15: Protein profile based on the gel image shown in Figure 20

Index	Protein Name	Accession #	Protein Mw	Protein pI	Peptide Count
1	Tumor rejection antigen-1 (gp96); glucose regulated protein, 94 k	gi|4507677	92411	4.76	26
2	Chaperone; heat shock 90kDa protein 1, beta	gi|20149594	83212	4.97	21
3	valosin-containing protein; yeast Cdc48p homolog; transitional endoplasmic reticulum ATPase	gi|6005942	89265	5.14	25
4	heat shock 70kDa protein 5 (glucose-regulated protein, 78kDa); BiP	gi|16507237	72288	5.07	21
5	thyroid hormone binding protein precursor	gi|339647	57068	4.82	6
6	Not identified				
7	prolyl 4-hydroxylase, beta subunit	gi|20070125	57080	4.76	23
8	N/I				
9	Chain A, Ribonuclease Inhibitor-Angiogenin Complex	gi|3892017	49810	4.71	6
10	vimentin [Homo sapiens]	gi|5030431	41537	4.82	17
11	Beta 5-tubulin [Homo sapiens]	gi|18088719	49639	4.75	19

12	tubulin alpha 6 [Homo sapiens]	gi|14389309	49863	4.96	18
13	protein disulfide isomerase-related protein 5	gi|1710248	46170	4.95	10
14	chaperonin containing TCP1, subunit 5 (epsilon) [Homo sapiens]	gi|24307939	59632	5.45	12
15	chaperonin containing TCP1, subunit 8 (theta)	gi|42662316	59582	5.42	10
16	keratin 8; cytokeratin 8; keratin, type II cytoskeletal 8 [Homo sapiens]	gi|4504919	53671	5.52	26
17	cytovillin 2	gi|340217	68119	5.8	7
18	ALDH3A1 protein [Homo sapiens]	gi|33871063	57473	6.96	10
19	chaperonin containing TCP1, subunit 2 (beta)	gi|5453603	57452	6.01	11
20	human rab GDI [Homo sapiens]	gi|285975	50631	5.94	13
21	eukaryotic translation elongation factor 1 gamma; elongation factor 1-gamma	gi|4503481	50087	6.25	9
22	proliferation-associated 2G4, 38kDa	gi|5453842	43785	6.13	14
23	Mitochondrial Aconitase 2 [Homo sapiens]	gi|20072188	85511	7.62	9
24	Far upstream element binding protein 1 (FUSE binding protein 1) (FBP) (DNA helicase V) (HDH V)	gi|37078490	67431	7.18	17
25	N/I				
26	uridine diphosphoglucose dehydrogenase	gi|7431380	55058	7.06	12
27	isocitrate dehydrogenase 1 (NADP+), soluble; oxalosuccinate decarboxylase	gi|28178825	46629	6.53	13
28	F-actin capping protein alpha-1 subunit; Cap Z	gi|5453597	32902	5.45	5
29	cytosolic inorganic pyrophosphatase	gi|11056044	32639	5.54	11
30	Chain A, Human Heart L-Lactate Dehydrogenase H Chain, Ternary Complex With Nadh And Oxamate	gi|13786847	36484	5.72	11
31	protein phosphatase 1, catalytic subunit, beta isoform 1; protein phosphatase 1, catalytic subunit,	gi|4506005	37162	5.84	5
32	transaldolase 1; dihydroxyacetone transferase; glycerone transferase [Homo sapiens]	gi|5803187	37516	6.36	11
33	annexin I; annexin I (lipocortin I); lipocortin I	gi|4502101	38689	6.57	13
34	poly(rC) binding protein 1; poly(rC)-binding protein 1 [Mus musculus]	gi|6754994	37473	6.66	5
35	heterogeneous nuclear ribonucleoprotein homolog JKTBP [imported] - human	gi|7446333	33568	6.85	6
36	esterase D/formylglutathione hydrolase; Esterase D; S-formylglutathione hydrolase	gi|33413400	31442	6.54	9
37	cytosolic malate dehydrogenase; soluble malate dehydrogenase [Homo sapiens]	gi|5174539	36403	6.91	5
38	aldo-keto reductase family 1, member B10; aldose reductase-like 1; aldo-keto reductase family 1	gi|20127592	35997	7.12	6
39	glyceraldehyde-3-phosphate dehydrogenase	gi|31645	36031	8.26	7
40	aldo-keto reductase [Homo sapiens]	gi|3493209	35996	7.67	7
41	nascent-polypeptide-associated complex alpha polypeptide [Homo sapiens]	gi|5031931	23369	4.52	5
42	14-3-3 gamma protein [Homo sapiens]	gi|5726310	28356	4.66	4
43	N/I				
44	chromobox homolog 3; heterochromatin protein HP1 gamma;	gi|15082258	20798	5.23	5
45	eukaryotic translation initiation factor 5A; eIF5AI [Homo sapiens]	gi|4503545	16821	5.08	2
46	dUTP pyrophosphatase [Homo sapiens]	gi|4503423	17736	6.15	8
47	thioredoxin peroxidase; thioredoxin peroxidase (antioxidant enzyme) [Homo sapiens]	gi|5453549	30520	5.86	9
48	glutathione-S-transferase omega 1; glutathione-S-	gi|4758484	27548	6.23	5

	transferase like; glutathione transferase omega				
49	peroxiredoxin 3 isoform b; antioxidant protein 1; thioredoxin-dependent peroxide reductase precursor	gi|32483377	25822	7.04	4
50	DJ-1 protein, DNA-binding protein regulatory subunit - human	gi|7429593	19834	6.33	10
51	Chain A, Horf6 A Novel Human Peroxidase Enzyme	gi|3318841	25011	6	12
52	proteasome alpha 1 subunit isoform 2;	gi|4506179	29536	6.15	12
53	phosphoglycerate mutase 1 (brain); Phosphoglycerate mutase A, nonmuscle form	gi|4505753	28785	6.67	6
54	Chain A, Ligand-Free Human Glutathione S-Transferase M1a-1a	gi|4388890	25564	6.28	6
55	Chain A, The Structure Of Holo Type Human Cu, Zn Superoxide Dismutase	gi|31615344	15794	5.7	3
56	N/I				
57	Crystal Structure Of A Human Low Molecular Weight Phosphotyrosyl Phosphatase.	gi|3891774	17899	6.35	6
58-62	N/I				
63	Cdc42 From Human, Nmr, 20 Structures	gi|2624582	21473	6.92	3
64-66	N/I				
67	Synovial sarcoma, X breakpoint 5, isoform a	gi|16741685	26266	9.61	8

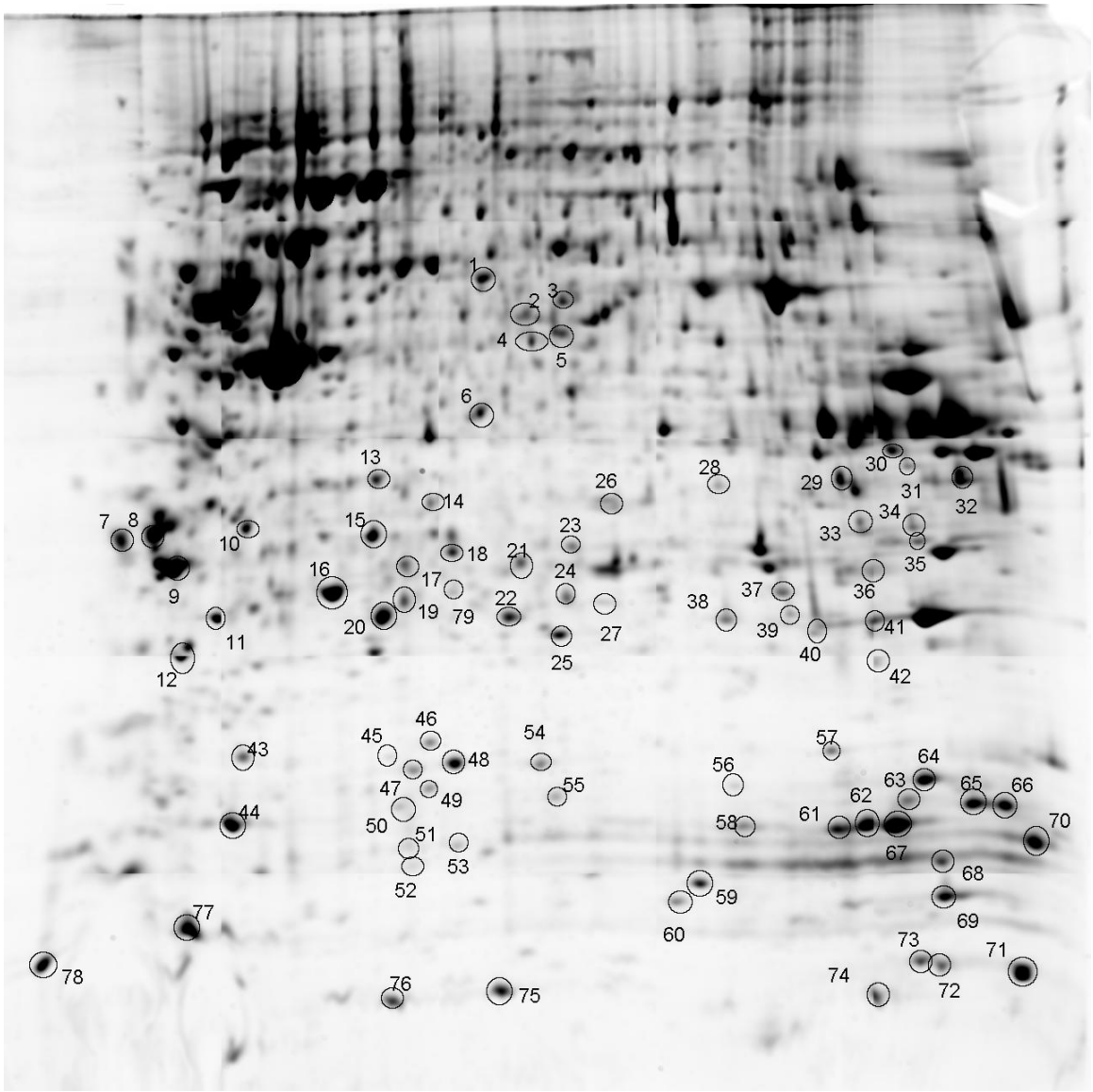

Figure 21: Protein distribution map of discodermolide-treated H460 human non-small cell lung cancer cells after electrophoresis in 17 cm gel

Table 16: Protein profile based on the gel image shown in Figure 21

Index	Protein Name	Accession #	Protein Mw	Protein pI	Peptide Count
1	heterogeneous nuclear ribonucleoprotein H1	gi|5031753	49198	5.89	11
2	Eukaryotic translation elongation factor 1 gamma [Homo sapiens]	gi|15530265	50115	**6.25**	7
3	GDP dissociation inhibitor 2; rab GDP-dissociation inhibitor, beta [Homo sapiens]	gi|6598323	50630	6.11	14
4	S-adenosylhomocysteine hydrolase	gi|178277	47684	6.03	10
5	annexin VII isoform 1; annexin VII (synexin); synexin [Homo sapiens]	gi|4502111	50283	6.25	7
6	protein phosphatase 1, catalytic subunit, beta isoform 1; protein phosphatase 1, catalytic subunit,	gi|4506005	37162	5.84	5
7	tat-associated protein	gi|1096067	30965	4.78	4
8	tyrosine 3/tryptophan 5 -monooxygenase activation protein, epsilon polypeptide; 14-3-3 epsilon; mit	gi|5803225	29155	4.63	12
9	tyrosine 3-monooxgenase/tryptophan 5-monooxgenase activation protein, gamma polypeptide; 14-3-3 pro	gi|9507245	28284.	4.8	12
10	chloride intracellular channel 1; p64CLCP; chloride channel ABP	gi|14251209	26905	5.09	2
11	N/I				
12	TCTP; tumor protein, translationally-controlled 1; fortilin; histamine-releasing factor [Homo sapiens]	gi|33285832	19581	4.98	7
13	inorganic pyrophosphatase; cytosolic inorganic pyrophosphatase; inorganic pyrophosphatase 1; pyroph	gi|11056044	32639	5.54	9
14	proteasome activator subunit 3 isoform 2; Ki nuclear autoantigen; Ki antigen; proteasome activator	gi|30410796	30867	5.79	12
15	prohibitin [Homo sapiens]	gi|4505773	29785	5.57	17
16	ubiquitin carboxyl-terminal esterase L1 (ubiquitin thiolesterase); Ubiquitin C-terminal esterase L1	gi|21361091	24808	5.33	13
17	proteasome beta-subunit - human	gi|631345	25892	5.7	5
18	thioredoxin peroxidase; thioredoxin peroxidase (antioxidant enzyme)	gi|5453549	30520	5.86	7
19	N/I				
20	glutathione S-transferase-P1c [Homo sapiens]	gi|726098	23355	5.43	8
21	N/I				
22	proteasome beta 3 subunit; proteasome theta chain; proteasome chain 13; proteasome component C10-II	gi|22538465	22933	6.14	10
23	endoplasmic reticulum protein 29 precursor; endoplasmic reticulum lumenal protein ERp28 [Homo sapiens]	gi|5803013	28975	6.77	9
24	proteasome beta 2 subunit; proteasome subunit, beta type, 2; macropain subunit C7-I; multicatalytic	gi|4506195	22821	6.51	6
25	Chain A, Crystal Structure Of The K130r Mutant Of Human Dj-1	gi|33358055	20970	6.5	7
26	Proteasome alpha 1 subunit, isoform 2 [Homo sapiens]	gi|13543551	29578	6.15	8
27	von Hippel-Lindau binding protein 1; VHL binding protein-1; prefoldin 3 [Homo sapiens]	gi|4507873	22611	6.63	7
28	esterase D/formylglutathione hydrolase; Esterase D; S-formylglutathione hydrolase	gi|33413400	31442	6.54	9
29	voltage-dependent anion channel 2 [Homo sapiens]	gi|42476281	31546	7.49	9
30	heterogeneous nuclear ribonucleoprotein A2/B1	gi|4504447	35983	8.67	12

	isoform A2; heterogeneous nuclear ribonucleoprotein B				
31	Annexin A2 [Homo sapiens]	gi|16306978	38593	7.57	18
32	Chain A, Crystal Structure Of Human Dt-Diaphorase (Nad(P)h Oxidoreductase)	gi|7766987	30659	8.91	7
33	proteasome alpha 4 subunit;PSMA4	gi|4506185	29465	7.57	7
34	Calcyclin binding protein	gi|45709259	26165	7.63	3
35	electron-transfer-flavoprotein, beta polypeptide	gi|4503609	27826	8.24	10
36	eukaryotic translation initiation factor 4H isoform 2	gi|14702180	25184	7.79	6
37	proteasome alpha 2 subunit ;PSMA2 protein	gi|39644890	24853	7.08	9
38	proteasome beta 2 subunit; proteasome subunit, beta type, 2; macropain subunit C7-I;	gi|4506195	22821	6.51	7
39	ATP synthase, H+ transporting, mitochondrial F1 complex, alpha subunit, isoform 1, cardiac muscle;	gi|4757810	59713	9.16	14
40	RAN protein [Homo sapiens]	gi|32425497	25206	7.16	5
41	biliverdin-IX beta reductase isozyme I {EC 1.3.1.24} [human, liver, Peptide, 204 aa]	gi|544759	21846	7.31	7
42	prostatic binding protein; phosphatidylethanolamine binding protein	gi|4505621	21043	7.01	5
43	eukaryotic translation initiation factor 5A; eIF5AI [Homo sapiens]	gi|4503545	16821	5.08	8
44	translation initiation factor eIF-4C - human	gi|1082871	16460	5.07	4
45	N/I				
46	dUTP pyrophosphatase	gi|4503423	17736	6.15	8
47	Chain A, X-Ray Structure Of Human Nucleoside Diphosphate Kinase A Complexed With Adp At 2 A Resolut	gi|37928159	17096	5.67	7
48	nucleoside-diphosphate kinase 1 isoform b [Homo sapiens]	gi|4557797	17137	5.83	7
49	Stathmin 1 [Homo sapiens]	gi|15680064	17325	5.76	2
50	N/I				
51	histone H3	gi|386772	15238	10.99	6
52	H2B histone family, member J	gi|4504269	13883	10.31	7
53	N/I				
54	Chain A, Structure Of Arf1-Gdp Bound To Sec7 Domain Complexed With Brefeldin A	gi|40889633	18788	5.63	4
55	prefoldin 2 [Homo sapiens]	gi|12408675	16637	6.2	5
56	N/I				
57	basic transcription factor 3; nascent-polypeptide-associated complex beta polypeptide [Homo sapiens	gi|20070130	17688	6.85	3
58	peptidylprolyl isomerase A; cyclophilin A [Mus musculus]	gi|6679439	17959	7.74	5
59	N/I				
60	40S ribosomal protein S12	gi|133742	14516	6.3	3
61	Chain A, Cyclophilin A Complexed With Cyclosporin A (Nmr, 22 Structures)	gi|1431788	17980	7.44	5
62	Peptidylprolyl isomerase A (cyclophilin A) [Homo sapiens]	gi|13937981	17999	7.68	11
63	destrin (actin depolymerizing factor) [Homo sapiens]	gi|5802966	18493	8.06	3
64	cofilin 1 (non-muscle) [Homo sapiens]	gi|5031635	18490	8.22	8
65	anterior gradient 2 homolog; secreted cement gland homolog; anterior gradient 2 homolog (Xenepus la	gi|5453541	19966	9.03	8
66	nucleoside-diphosphate kinase 2; non-metastatic cells 2, protein (NM23) expressed in; c-myc transcr	gi|4505409	17286	8.52	3

67	Chain A, Cyclophilin A	gi|1633054	17869	7.82	6
68	Chain A, Human Mitochondrial Single-Stranded Dna Binding Protein	gi|2624694	15185	8.23	10
69-70	N/I				
71	Putative S100 calcium-binding protein H_NH0456N16.1	gi|13431875	11501	8.83	2
72	Chain A, Macrophage Migration Inhibitory Factor (Mif) With Hydroxphenylpyruvate	gi|5542151	12337	8.24	2
73	S100 calcium-binding protein A10; S100 calcium-binding protein A10 (annexin II ligand, calpactin I,	gi|4506761	11195	6.82	3
74	dJ908M14.1.3 (ribosomal protein S21, isoform 3) [Homo sapiens]	gi|12964241	9887	7.71	2
75	S100 calcium-binding protein A4; S100 calcium-binding protein A4 (calcium protein, calvasculin, met	gi|4506765	11720	5.85	4
76	N/I				
77	Thioredoxin (Reduced Form)	gi|230939	11699	4.82	3
78	Chain D, Crystal Structure Of Edema Factor Complexed With Calmodulin	gi|18655708	16268	4.11	4
79	Eukaryotic translation initiation factor 4E	gi|15214959	25080	6	1

3. FUTURE PLANS

3.1. PROTEIN SAMPLE FRACTIONATION

In the current experiments, 17 cm pH 3-10, non-linear IPG strips were used in isoelectric focusing and 183 × 193 × 1 mm Tris-HCl gel for second dimension separation. One of two spots that were found to have an expression level change is stathmin. As seen in the mass spectrum shown in Figure 15, a pair of ions at *m/z* 1388.7/1294.3 represents a phosphopeptide (15-27) with the sequence *ASGQAFELILSPR*. It is not known yet which serine is phosphorylated within this sequence. Interestingly, no other phosphorylated stathmin isoforms were detected. Muller, *et al.* reported a mass spectrometric method, which characterized stathmin isoforms separated on 2D PAGE. In their experiments, a pH 4-7 linear IPG strip were soaked in sample solution and a 20 × 25 cm SDS-PAGE gel was used to run second dimensional electrophoresis overnight. Multiple isoforms of phosphorylated stathmin were identified from the Coomassie Brilliant Blue G250 stained gel (Figure 22) [63]. This result provides a good example and is encouraging. In future experiments, a narrow range IPG strip will be used to exclude excessive information while expanding the region of interested.

3.2. SATURATION LABELING

To avoid the gel-to-gel variation in traditional 2D PAGE, 2D DiGE was employed in the present experiments. Two mass and charge-matched cyanine dyes (Cy3 and Cy5) were used in a minimal labeling manner. Even as the dyes undoubtedly offer benefits to image analysis, there

are a few limitations due to the nature of the labeling reaction. Firstly, the dye to protein ratio is kept deliberately low (less than 5%) in order to avoid multiple dye additions on each protein molecule, which would lead to more than one spot per protein on a 2D gel. Due to the high lysine content of most proteins (e.g., 10.1% across eight random proteins [64]) it would be difficult to force the labeling reaction to saturation without the need for excessive amounts of dyes. Therefore, the sensitivity of the minimal labeling dyes could be further enhanced. Secondly, the fact that less than 5% of protein is labeled means that the unlabeled bulk runs with a higher mobility because the dye itself has a mass of 434-464 Da. This will make precise spot excision a problem in practice. Post-staining is necessary to match spots on the images. To improve the sensitivity and to overcome the problem in spot picking, a new labeling strategy is proposed to use which allows the saturated labeling on an alternative, less prevalent amino acid residue. Cysteine is one of such residues which are about 2.47% across eight random proteins [64]. The reactive thiol group of cysteine reacts with maleimide through nucleophilic addition to form a thioester (Figure 23) [65]. We could try in the future two kinds of new maleimide cyanine dyes commercially available from Amersham Biosciences.

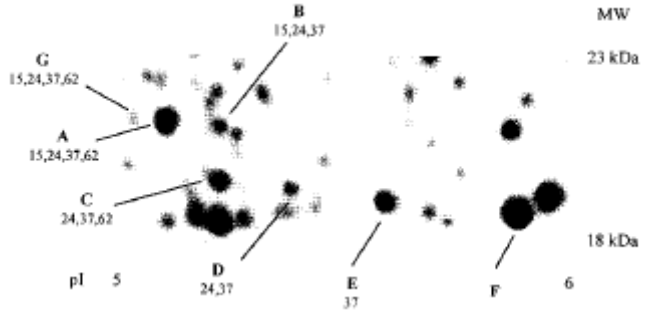

Figure 22: 2D PAGE separation of stathmin isoforms with major phosphorylated components indicated. In this case IEF was performed on linear pH 4-7 IPG strips [excerpted from Müller et al., ref. 63].

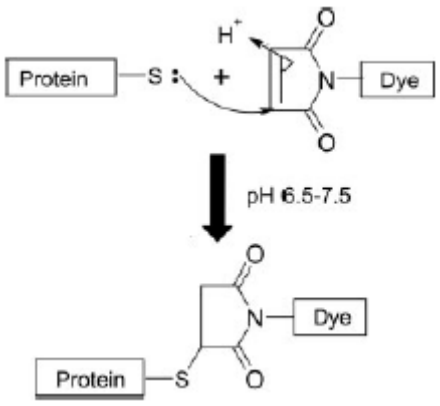

Figure 23: Schematic of labeling reaction of protein thiols with maleimide cyanine dyes [excerpted from Shaw et al., ref. 65].

3.3. APPLICATION OF HPLC TO PROTEIN MIXTURE SEPARATION AND PROTEIN IDENTIFICATION

Even though samples were carefully handled in all steps of labeling, separation and tryptic digestion, there were still a large number of spots that could not be identified successfully. These spots might be of small amounts (5-25 μg) or have a mixture of multiple peptides, which leads to unsolved problem in database search. The researchers at Applied Biosystems have recently developed a simple step elution-based 2-D peptide chromatography setup. This facility consists of an UltiMate nano HPLC system (Dionex), a FAMOS autosampler (Dionex) and a Probot microfraction collector (Dionex) and features an increased sample loading capacity and resolving power. By using this LC-MALDI approach, intermediate amounts (5-25 μg) of complex proteomic samples can be separated into multiple fractions and each fraction can further be washed off as continuous tiny droplets, which are then spotted on MALDI plates. Database searching with different available software, e.g., Sequest from ThermoFinnigan, may be useful in the identification of protein samples when data from all fractions is combined.

3.4. POTENTIAL TARTETS THAT MIGHT HAVE PROTEOMIC CHANGES

Two strategies are currently employed in the exploration of proteomic changes. The passive strategy is to run 2-D electrophoresis followed by image analysis. While on the other hand, the active strategy is to adjust and optimize the experimental design to the predicted targets to see if there really exist some changes. As the depth of this project increases, an intentional move toward the active strategy can be made based on the accumulated data and knowledge. As microtubule stabilization proceeds toward arrest at the G2/M phase and further the induction of apoptosis, it could be assumed that proteins associated with cell cycle and microtubule dynamics should have some proteomic changes, either in expression or in post-translational modification. As mentioned previously, microtubule-servering associated with unregulated EEF1A may be a contributor to the cell death [59]. Thus, EEF1A could be one of the next targets to which attention should be paid. Another target would be microtubule associated proteins (MAPs) because they are in intimate relation with microtubule dynamics. In addition, the accumulating evidence has suggested that molecular changes including overexperssion of oncogenes and decreased expression of tumor suppressor genes are responsible for lung carcinogenesis [66]. Liu, Y. et al. has compared the protein expression changes of human non-small cell lung cancer (NSCLC) cell lines with normal human bronchial epithelial cell lines [67]. Eight proteins including EEF1Bβ, vimentin, cytokeratin 8, YB-1, PCNA, Nm23, hnPNP A2/B1, and HSP90β were found to up-regulated in lung cancer cells, and the tumor suppressor protein 14-3-3σ was found to be down-regulated. Chang, et al. also reported a comparison study, in which antioxidant enzyme peroxiredoxin I was identified to be overexpressed because of the continuous exposure of human lung to oxidative stress. Obviously, these proteins should be taken into consideration in subsequent studies.

BIBLIOGRAPHY

1. Gudkov, A. V., *Cancer drug discovery: the wisdom of imprecision*. Nature Medicine, 2004. **10**(12): p. 1298-99.

2. Issaeva, N. et al. *Small molecule RITA binds to p53, blocks p53–HDM-2 interaction and activates p53 function in tumors*. Nature Medicine, 2004. **10**(12): p. 1321–28

3. Kumar, N. *Taxol-induced polymerization of purified tubulin. Mechanism of action*. J Biol Chem, 1981. **256**: p. 10435-41

4. Mollinedo, F., Gajate, C., *Microtubules, microtubule-interfering agents and apoptosis*. Apoptosis, 2003. **8**(5): p. 413-50

5. Mitchison, T. J., Kirschner, M., *Dynamic instability of microtubule growth*. Nature, 1984. **312**: p. 237-42

6. Margolis, R. L., Wilson, L. *Microtubule treadmilling: what goes around comes around*. Bioessays, 1998. **20**: p. 830-36

7. Jordan, M. A., *Mechanism of action of antitumor drugs that interact with microtubules and tubulin*. Curr Med Chem Anti-Canc Agents, 2002. **2**: p. 1-17

8. Rowinsky, E. K., et al., *Taxol: the first of the taxanes, an important new class of antitumor agents*. Semin Oncol, 1992. **19**(6): p. 646-62.

9. Eckardt, J. R., *Antitumor activity of docetaxel*. Am J Health Syst Pharm, 1997. **54**(24 Suppl 2): p. S2-6.

10. Neuss, N., et al., *Vinca alkaloids XXXIII [1]. Microbiological conversions of vincaleukoblastine (VLB, vinblastine), an antitumor alkaloid from Vinca rosea*. Linn. Helv Chim Acta, 1974. **57**(6): p. 1886-1890.

11. ter Haar, E., et al., *Discodermolide, a cytotoxic marine agent that stabilizes microtubules more potently than taxol*. Biochemistry, 1996. **35**(1): p. 243-250.

12. Mandelkow, E., et al., *Microtubules and microtubule-associated proteins*. Curr Opin Cell Biol, 1995. **7**: p. 72-81

13. Ookata, K., et al., *Cyclin B interaction with microtubule-associated protein 4 (MAP4) targets p34cdc2 kinase to microtubules and is a potential regulator of M-phase microtubule dynamics*. J Cell Biol, 1995. **128**(5): p. 849-62

14. Khayat, D., Antoine, E. C., Coeffic, D., *Taxol in the management of cancers of the breast and the ovary*. Cancer Invest, 2000. **18**: p. 242-60

15. Calderoni, A., Cerny, T., *Taxanes in lung cancer: a review with focus on the European experience*. Crit Rev Oncol Hematol, 2001. **38**: 105-27

16. Balachandran, R., ter Haar, E., Welsh, M. J., Grant, S. G., Day, B. W., *The potent microtubule-stabilizing agent (+)-discodermolide induces apoptosis in human breast carcinoma cells—preliminary comparisons to paclitaxel*. Anti-Cancer Drugs, 1998. **9**: p. 67-76

17. Mooberry, S. L., Tien, G., Hernandez, A. H., Plubrukarn, A., Davidson, B. S., *Laulimalide and isolaulimalide, new paclitaxel-like microtubule-stabilizing agents.* Cancer Res,1999. **59**: p. 653-60

18. Peettit, G. R., Cichacz, Z. A., Isolation and structure of dictyostatin 1. US Patent No. 5,430,053, 1995

19. Pettit, G. R., Cichacz, Z. A., et al., *Isolation and structure of the cancer cell growth inhibitor dictyostatin 1*. J Chem. Soc Chem Commun, 1994. **1994**: p. 1111-2

20. Bollag, D. M., et al., *Epothilones, a new class of microtubule-stabilizing agents with a taxol-like mechanism of action*. Cancer Res, 1995. **55**: p. 2325-33

21. Long, B. H., et al., *Eleutherobin, a novel cytotoxic agent that induces tubulin polymerization, is similar to paclitaxel (Taxol)*. Cancer Res, 1998. **58**: p. 1111-15

22. Pryor, D. E., et al., *The microtubule stabilizing agent laulimalide does not bind in the taxoid site, kills cells resistant to paclitaxel and epothilones, and may not require Its epoxide moiety for activity*. Biochemistry, 2002. **41**: p. 9109-15

23. Schiff, P. B., Horwitz, S. B., *Taxol stabilizes microtubules in mouse fibroblast cells*. Proc Natl Acad Sci USA, 1980. **77**: p. 1561-65

24. Derry, W., Wilson, L., Jordan, M. A., *Substoichiometric binding of Taxol suppresses microtubule dynamics*. Biochemistry, 1995. **34**: p. 2203-11

25. Rao, S., et al., *3'-(p-azidobenzamido)taxol photolabels the N-terminal 31 amino acids of beta-tubulin*. J Biol Chem, 1994. **269**: p. 3132-34

26. Rao, S., et al., *Characterization of the Taxol Binding Site on the Microtubule*. J Biol Chem, 1995. **270**: 20235-38

27. Nogales, E., et al., *Structure of the $\alpha\beta$ tubulin dimer by electron crystallography*. Nature, 1998. **391**: p. 199-203

28. Nogales, E. et al., *High-Resolution Model of the Microtubule*. Cell, 1999. **96**: p. 79-88

29. Kowalski, R. J., et al., *The microtubule-stabilizing agent discodermolide competitively inhibits the binding of paclitaxel (Taxol) to tubulin polymers, enhances tubulin nucleation reactions more potently than paclitaxel, and inhibits the growth of paclitaxel-resistant cells*. Mol Pharmacol, 1997. **52**: p. 613-22

30. Kowalski, R. J., Giannakakou, P., Hamel, E., *Activities of the microtubule-stabilizing agents epothilones A and B with purified tubulin and in cells resistant to paclitaxel (Taxol)*. J Biol Chem, 1997. **272**: p. 2534-41

31. Martello, L. A., et al., *Taxol and Discodermolide Represent a Synergistic Drug Combination in Human Carcinoma Cell Lines*. Clin Cancer Res, 2000. **6**: p. 1978-87

32. Shin, Y., et al., *Discodermolide/dictyostatin hybrids: synthesis and biological evaluation*. Org Lett, 2002. **4**: p. 4443-46

33. Barltrop, J. A. and Owen, T. C., *5-(3-carboxymethoxyphenyl)-2-(4,5-dimenthylthiazolyl)-3-(4-sulfophenyl)tetrazolium, inner salt (MTS) and related analogs of 3-(4,5-dimethlythiazolyl)-2,5-diphenyltetrazolium bromide (MTT) reducing to purple water-soluable formazans a cell-viability indicators*. Bioorg & Med Chem Lett, 1991. **1**(11): p. 611

34. Berridge, M. V. and Tan, A. S., *Characterization of the cellular reduction of 3-(4,5-dimethlythiazol-2-yl)-2,5-diphenyltetrazolium bromide (MTT): subcellular localization, substrate dependence, ad involvement of mitochondrial electron transport in MTT reduction*. Arch Biochem Biophys, 1993. **303**(2): p. 474-82

35. Cory, A. H., et al., *Use of an aqueous sobuble tetrazolium/formazan assay for cell growth assays in culture*. Cancer Commun, 1991. **3**(7): p. 207-12

36. Löwe, J., et al., *Refined structure of $\alpha\beta$-tubulin at 3.5 Å resolution*. J Mol Biol, 2001. **313**: p. 1045-57

37. Isbrucker, R. A., et al., *Tubulin polymerization activity of dictyostatin-1, a polyketide of marine sponge origin*. Biochem Pharmacol, 2003. **66**: p. 75-82

38. Pusztai, L., et al., *Pharmacoproteomic analysis of prechemotherapy and postchemotherapy plasma samples from patients receiving neoadjuvant or adjuvant chemotherapy for breast carcinoma*. Cancer, 2004. **100**: p 1814-22

39. Unlu, M., Morgan, M. E., Minden, J.S., *Difference gel electrophoresis: a single gel method for detecting changes in cell extracts*. Electrophoresis, 1997. **18**: p. 2071-2077

40. Schuler, Benjamin and Pannell, Lewis K., *Specific labeling of polypeptides at amino-terminal cysteine residues using Cy5-benzyl thioester*. Bioconjugate Chem, 2002. **13**: p. 1039-1043

41. Tonge, R., et al., *Validation and development of fluorescence two dimensional differential gel electrophoresis proteomics technology*. Proteomics, 2001. **1**(3): p. 377-96

42. Marie, E. B., et al., *Proteomic characterization of harvested pseudopodia with differential gel electrophoresis and specific antibodies*. Laboratory Investigation, 2005. p. 1-12

43. Bradford, M. M., Anal Biochem, 1976. **72**: p. 248

44. Laemmli, U. K., *Cleavage of structural proteins during the assembly of the head of bacteriophage T4*. Nature, 1970. **227**: p. 680-85

45. Kreil, D. P., et al., *DNA microarray normalization methods can remove bias from differential protein expression analysis of 2D difference gel electrophoresis results*. Bioinformatics, 2004. **20**(13): p. 2026-34

46. Roepstorff, P., *Mass spectrometry in protein studies from genome to function*. Curr Opin Biotechnol, 1997. **8**(1): p. 6-13.

47. Karas, M. and F. Hillenkamp, *Laser desorption ionization of proteins with molecular masses exceeding 10,000 daltons*. Anal Chem, 1988. **60**(20): p. 2299-301.

48. Pappin, D. J., P. Hojrup, and A.J. Bleasby, *Rapid identification of proteins by peptide-mass fingerprinting*. Curr Biol, 1993. **3**(6): p. 327-32.

49. Lawler, Sean, *Microtubule dynamics: If you need a shrink try stathmin/Op18*. Current Biology, 1998. **8**: p. 212-14

50. Sobel, A, *Stathmin: a relay phosphoprotein for multiple signal transduction?* Trends Biochem Sci, 1991. **16**: p. 301-05

51. Melander Gradin H., el al. *Regulation of microtubule dynamics by extracellular signals: cAMP-dependent protein kinase switches off the activity of oncoprotein 18 in intact cells*. J Cell Biol, 1998. **140**: p. 131-41

52. DiPaolo, G., et al. *Phosphorylation regulates the microtubule-destabilizing activity of stathmin and its interaction with tubulin*. FEBS Lett, 1997. **416**: p. 149-52

53. Larsson, N., et al. *Control of microtubule dynamics by oncoprotein 18: dissection of the regulatory role of multisite phosphorylation during mitosis*. Mol Cell Biol, 1997. **17**: p. 5530-39

54. Mistry, S. J. and Atweh, G. F., *Role of stathmin in the regulation of the mitotic spindle: potential applications in cancer therapy*. Mount Sinai J Med, 2002. **69**(5): p. 299-304

55. Thornton, S., et al., *Not just for housekeeping: protein initiation and elongation factors in cell growth and tumorgenesis*. J Mol Med, 2003. **81**: p. 536-48

56. Shiina, N., et al., *Microtubule servering by elongation factor 1α.* Science, 1994. **266**: p. 282-85

57. Shiina, N., et al., EMBO J, 1992. **11**: p. 3977

58. Shiina, N., et al., *Tyrosine phosphorylation by the epidermal growth factor receptor kinase induces functional alterations in microtubule-associated protein* **2** J Biol Chem, 1987. **262**: p. 16200-204

59. Kato, M. V., et al., *Upregualtion of the elongation factor-1α gene by p53 in association with death of an erythroleukemin cell line*. Blood, 1997. **90**(4): p. 1373-78

60. Potter, M., et al., *The wst gene regulates multiple forms of thymcyte apoptosis*. Cell Immunol, 1998. **188**: p. 111-17

61. Talapatra, S., el al., *Elongation factor-1 alpha is a selective regulator of growth factor withdrawal and ER stress-induced apoptosis*. Cell Death Differ, 2001. **9**: p. 856-61

62. Ruest, L. B., et al., *Peptide elongation factor eEF1A-2/S1 expression in cultured differentiated myotubes and its protective effect against caspase-3-mediated apoptosis*. J Biol Chem, 2002. **277**: p. 5418-25

63. Müller, D. R., et al. *Mass spectrometric characterization of stathmin isoforms separated by 2D PAGE*. J Mass Spectrom, 1999. **34**: p. 336-45

64. Lehninger, A. L., *Biochemistry*, Worth Publishers, New York, 1971, p. 94

65. Shaw, J., et al. *Evaluation of saturation labeling two-dimensional difference gel electrophoresis fluorescent dyes*. Proteomics, 2003. **3**: p. 1181-95

66. Osada, H., and Takahashi, T., *Genetic alterations of multiple tumor suppressors and oncogenes in the carcinogenesis and progression of lung cancer.* Oncogene, 2002. **21**: p. 7421-34

67. Liu, Y., Chen, Q., Zhang, J.-T., *Tumor suppressor gene 14-3-3σ is down-regulated whereas the proto-oncogene translation elongation factor 1δ is up-regulated in non-small cell lung cancers as identified by proteomic profiling.* J Proteome Res, 2004**.** **3**(4): p. 728-735